Journal of
ALLOYS
AND COMPOUNDS

Structural Investigation of Mechanically Activated ZnO powder

A. Peleš, V.P. Pavlović, S. Filipović, N. Obradović, L. Mančić, J. Krstić, M. Mitrić, B. Vlahović, G. Rašić, D. Kosanović, V.B. Pavlović

PII: S0925-8388(15)30364-9
DOI: 10.1016/j.jallcom.2015.06.247
Reference: JALCOM 34655

To appear in: *Journal of Alloys and Compounds*

Received Date: 22 January 2015
Revised Date: 20 June 2015
Accepted Date: 27 June 2015

Please cite this article as: A. Peleš, V.P. Pavlović, S. Filipović, N. Obradović, L. Mančić, J. Krstić, M. Mitrić, B. Vlahović, G. Rašić, D. Kosanović, V.B. Pavlović, Structural Investigation of Mechanically Activated ZnO powder, Journal of Alloys and Compounds (2015), doi: 10.1016/j.jallcom.2015.06.247.

This is a PDF file of an unedited manuscript that has been accepted for publication. As a service to our customers we are providing this early version of the manuscript. The manuscript will undergo copyediting, typesetting, and review of the resulting proof before it is published in its final form. Please note that during the production process errors may be discovered which could affect the content, and all legal disclaimers that apply to the journal pertain.

*Manuscript
Click here to view linked References

Structural Investigation of Mechanically Activated ZnO powder

A. Peleš[1], V. P. Pavlović[2], S. Filipović[1], N. Obradović[1], L. Mančić[1], J. Krstić[3], M. Mitrić[4], B. Vlahović[5], G. Rašić[5], D. Kosanović[1], V. B. Pavlović[1]

[1]Institute of Technical Sciences of SASA, Knez Mihailova 35/IV 11000 Belgrade, Serbia

[2]Faculty of Mechanical Engineering, University of Belgrade, 11000 Belgrade, Serbia

[3]Institute of Chemistry, Technology and Metallurgy, University of Belgrade, Njegoševa 12, 11000 Belgrade, Serbia

[4]Institute of Nuclear Sciences Vinca, Laboratory of Solid State Physics, 11001 Belgrade, Serbia

[5]North Carolina Central University, Durham, North Carolina 27707, USA

Abstract

Commercially available ZnO powder was mechanically activated in a planetary ball mill. In order to investigate the specific surface area, pore volume and microstructure of non-activated and mechanically activated ZnO powders the authors performed N_2 physisorption, SEM and TEM. Crystallite size and lattice microstrain were analyzed by X-ray diffraction method. XRD patterns indicate that peak intensities are getting lower and expend with activation time. The reduction in crystallite size and increasing of lattice microstrain with prolonged milling time were determined applying the Rietveld's method. The difference between non-activated and the activated powder has been also observed by X-ray photoelectron spectroscopy (XPS). XPS is used for investigating the chemical bonding of ZnO powder by analyzing the energy of photoelectrons. The lattice vibration spectra were obtained using Raman spectroscopy. In Raman spectra some changes along with atypical resonant scattering were noticed, which were caused by mechanical activation.

Keywords: Mechanical activation, N_2 physisorption, XRD, XPS, SEM, TEM, Raman spectroscopy, ZnO

1. Introduction

Due to its wide direct band gap (3.37eV) and large excitation binding energy at room temperature, ZnO is a very good semiconductor material and an important ceramic material for application in gas sensors, catalysis, solar cells and transducers. [1-6]. With its wurtzite structure improved ZnO characteristics, such as smaller and more uniformed particle size, are desirable properties for its application in multilayer ceramic capacitors and varistor, as well [7]. It is well known that the structural, morphological, and electronic properties of ZnO particles depend not only on the specific crystal structure, composition, and morphology of the oxide particles, but also on defect in their structure [8]. A nanosized powder with uniformed particle size distribution and controlled particle morphology is highly desirable.

There are many methods which can produce this type of powder such as microemulsions, colloidsynthesis routes, sol–gel methods and spray pyrolysis, ion implentation, laser ablation etc. for the preparation of various nanostructures and homogenization [1]. Among these methods, to produce nanocristalline powder and to improve the functional properties, mechanical activation has been employed, due to its simplicity, shortened time of sample preparation and low-cost.

Mechanical activation processes are used to modify the properties of materials, to enhance the reactivity of materials and to produce advanced materials etc. The reactivity of materials is dependent on different parameters such as activation time (duration time of milling process of powder) and type of energy mill. Also the different atmosphere, where the milling process is performed, has a big influence on reactivity of the material. Mechanical activation by grinding, as a method for modifying the physical and chemical properties of powder materials, is often used in powder technology [9, 10]. Specific changes that occur during grinding have a great influence on final properties of the obtained material, also improving their specific application. Mechanical activation by grinding requires a few processes and mainly occurs in four stages. In the first stage there is a destruction of material than in the second stage it can be observed a formation of a new surface on the material which is destroyed. Next stage is fine grinding and finally transformation into a new material with a different structure and properties [11]. Grinding could be performed in various types of mills such as ball-mill, planetary-mill vibratory mill, pin mill etc. High-energy milling process is one of the very powerful techniques for synthesizing and particles fragmentation of all kinds of materials [12, 13]. This method is widely used and it is continue to attract the serious attention of researchers.

Investigations of possible modifications of material properties are of vide interest, such as scientific and practical. A complex analysis of activated powders is necessary and requires complete information on the fine defect structure.

The goal of this research was to investigate the change in the structural characteristics of ZnO powder particles before and after milling process for shortened time (up to 30 minutes).

2. Experimental procedure

Commercially available ZnO powder (Sigma Aldrich, 99.9% p.a.) was mechanically activated by grinding in a high-energy planetary ball mill (Fritsch Pulverisette 7) at air atmosphere. We used wolfram carbide balls, with 5 mm in diameter, while powder to ball mass ratio was 40:1. Activation time for this study was 5, 10 and 30 minutes. Measurements of specific surface area and pore volume of non-activated and mechanically activated powders were carried out using Sorptomatic 1990 Thermo Electron device. Data processing was performed using the software package Advanced Data Processing Version 5.1 Realese 5.13.

The microstructure morphology of all powders has been investigated using scanning electron microscopy (JEOL JSM-6390 LV) and Transmission electron microscopy (TEM, JEOL-100CX) .

X-ray diffraction patterns of the initial and activated powders were obtained on a Philips PW-1050 diffractometer with λCu-K_α radiation and a step/time scan mode of $0.05^o/5$ s. Structural refinements were carried out using the Rietveld′s method.

XPS analyses were performed using a Kratos Axis Ultra XPS system with Monochromated Aluminum K-Alpha X-Rays. The chamber vacuum during measurement was at 2.5 x10-8 torr. The X-Ray gun was operated at 15kW and 10mA. A charge neutralizer was used to reduce charging effects from non-conducting surfaces. Electrons were collected at 90 degrees from the sample surface. All survey scans were collected with a Pass Energy of 160eV and 1 sweep (or averaging). All Region scans were performed with a Pass Energy of 20eV. All data was calibrated to the C-C portion of the C1s peak at 284.5eV.

Raman scattering was performed by a He-Ne laser in three different wavelengths. An 1800 lines/inch grating was used. The data was collected using a count time of 5 seconds with 5 averaging cycles. The samples were measured under a microscope using a 100x objective.

3. Results and discussion

It is well known that mechanical activation leads to a decrease in crystallite size, appearance of structural defects, phase transformations, order-disorder transitions, amorphisation, chemical reactions, etc. [3, 13]. During the formation of mechanically activated nanocrystalline powders, in a size reduction process, powder particles brake in dependence on the applied stress and material properties [13]. The changes of the powder particle morphology and powder porosity appear during mechanical activation, manifested by interparticles void and pores within individual particles. Those changes can be analyzed by measuring pore volume and specific surface area. Our investigations showed that mechanical activation caused a significant increase in pore volume of ZnO powder. Changes in pore volume and specific surface area are shown in Fig. 1.

Applied mechanical activation introduces mechanical energy into the system, destroying the crystal structure of ZnO powder, increase the number of pores in the total porosity. Mechanical activation also changed the specific surface area. At the beginning, non-activated powder has specific surface of 6.9 m^2/g. After 5 minutes of activation, its value decreases to 5.9 m^2/g which is probably caused by powder particle adhesion. With prolonged milling time, values of specific surface area are increasing up to 7.8 m^2/g. These effects could be attributed to powder particle breakage, followed by increase in mesopore volume.

TEM analysis showed that the particles of non activated ZnO have polygonal shape, with smooth and uniform surfaces. As a result of mechanical activation the erosion of the surface occured as well as diminution of the particles. It has been also noticed that for the samples activated for 30 minutes increased surface activity influenced the formation of agglomerates, as it can be seen in figure 2.

The mechanical activation led to decrease in cristallite size, increase in microstrain, introducing the energy into the system. All that changes can be observed by lowering the intensities of XRD peaks as well as its broadening. Depending on activation time these changes have been study by performing XRD, XPS and Raman analysis.

Scanning electron micrographs are in accordance with data obtained by N_2 physisorption and TEM analysis.

Fig. 3. represents SEM micrographs of non-activated ZnO powder and powders activated for 5, 10 and 30 minutes. Initial non-activated ZnO is a submicron powder composed of particles 0.2-0.7 microns in size with clear boundaries between the grains. A high degree of anisotropy in the shape and form of a large number of needle-shaped particles is observed. Micrograph b) and c) show that with prolonged milling time particles gained uniformed distribution, while after 30 minutes of activation, formation of agglomerates approximately 1 micron in size, is noticed.

The size of particles accumulated on the agglomerates surface decreases with activation time. These results are given in the Table I. At the beginning, the size covered the range between 200 and 700 nm, while with the prolonged milling time, the particle size was in the range between 60 and 470 nm.

Soft agglomerates at the surface often form in mechanically activated powders as a result of increased surface energy of mechanically activated powders. It should be notice that the formations of agglomerations during the mechanical activation can have a negative impact on sintering process to get a ceramics with good performance. The agglomeration of nanoscaled powders in general decreases the density of green bodies pressed from those nanopowders. H. Ferkel and R.J. Hellmig showed in their work that a short ball-milling procedure decreases the amount of strong agglomerates in alumina and zirconia nanopowders produced with PVS and laser ablation technique [14]. In order to reduce powder agglomeration we chose the shortened time of activation, which have so far not been taken into consideration for ZnO powder.

Fig 4. represents XRD patterns of non-activated ZnO powder and the activated ones. The identification of obtained peaks has been performed using the ICSD card #82028 for ZnO. The tree most intensive peaks at 2θ = 31.74°, 34.38°, 36.22 were assigned to (100), (002) and (101) reflections of ZnO, indicating that samples were polycrystalline wurtzite structure.

Mechanical energy that introduces into the system by mechanical activation consumes an integral phase fragmentation and distortion of the crystal structure of the starting ZnO, as well as the increase of microstrain. At the beginning, large crystallites of non-activated ZnO, XRD patterns indicated sharp peaks intensities, but with prolonged milling time, those peaks intensities are getting lower along with their broadening. This may be explained by destabilization of the crystalline phase, particle refinement and crystallite size and generation of stress field [13]. This changes in peak intensity and their broadening is related to particle fragmentation and amorphization.

A process of mechanical activation is intense and energetically favorable for the producing defects within the structure. Such treatment of the powder leads to a significant increase in defects such as vacancies, dislocations, grain boundaries and they lead to change of lattice parameters and unit cell volume observed by Rietveld's method (Tab. II).

X-ray powder diffraction (XRPD) patterns of the initial and activated powders were obtained on a Philips PW-1050 diffractometer with λCu-Kα radiation and a step/time scan mode of 0.05°/5 s.

Lattice parameters (a, c) and volume of the ZnO unit cell ($V = \frac{\sqrt{3}}{2}a^2c$) were refined from the XRPD patterns by the Rietveld method using TOPAS 4.2 software. The space group P63mc (No.186) was used as a model, with the starting values of lattice parameters and atomic positions adopted from ICSD 82028. To achieve the best fit of experimental data Fundamental Parameter Approach was applied [15]. Peak shapes, lattice parameters, and scale were refined simultaneously. After convergence, atomic positions and isotropic temperature factors were included in the refinement. Calculation of the volume weighted mean crystallize sizes, based on the individual crystallite size (D) and strain (e_{hkl}) contributions to the peak profile shapes versus 2θ (a convolution of Lorentz and Gauss functions), was done using Double-Voigt approach. Size-broadening anisotropy in whole powder pattern fitting was described by spherical harmonics. The quality of the Rietveld refinement was evaluated in terms of the discrepancy factor profile weighted residual error (Rwp < 10%) and the Goodness-of-Fit indicator (GoF ~ 1).

The influence of applied mechanical activation on crystallite size reducing and increasing of microstrain is observed. Crystallite size decreases with activation time from 60.7 nm, for non-activated powder, to 35 nm for 30 minutes of activation. Also, the increase of microstrain is observed, from 0.0001 % for non-activated powder to 1.15 % for the powder activated for 30 minutes. Crystallite size decreases with prolonged milling time, while lattice strain increases. (Fig. 5).

XPS was used to study the electronic structure of the samples. The representative XPS spectra of O 1s and Zn 2p photoelectron lines are shown on Fig 6.

For non activated ZnO Zn2p core level spectrum comprises of a doublet Zn 2p 3/2 and Zn 2p 1/2 with symmetrical features, which rules out the presence of multi-omponent Zn. The doublet was fitted with two Gaussian peaks centered at 442,543 and 465,843 eV as shown in Fig. 6a, con firming the Zn^{2+} state. For the samples activated for 5 minutes, the main core level XPS spectrum of Zn 2p centered at ~ 442,186 eV and ~ 465,386 eV showed slightly asymmetrical features, indicating the existence of Zn in its multiple-oxidation states. The deconvoluted Zn 2p3/2 core level XPS spectrum shows two peaks, centered at ~ 465,432 eV and ~ 442,432 eV, for the samples activated for 10 minuters, and at at ~ 465,375 eV and ~ 442,175 eV, for the samples activated for 30 minutes, corresponding to different oxidation states of Zn. The lower energy peak in the deconvoluted spectrum is attributed to the Zn^{2+} ion array surrounded by O^{2-} ions in the hexagonal ZnO and is termed as the oxide form of Zn. The deconvoluted peak centered at the higher binding energy side is related to metallic zinc. This observation is in agreement with the XPS study of ZnO:Mn nanoparticle thin films performed by U. Ilyas et al. [16], as well as with Y.Y.Chen et al. [17].

As it can be seen from the the fit results of the O1s core level XPS spectra for non activated ZnO, the O 1s spectrum consists of the main peak O_I and subpeak O_{II}.The main O 1s peak O_I is attributed to O^{2-} bonded to Zn^{2+} and the subpeak O_{II} is related to OH group absorbed onto the surface of the ZnO particles . Beside those two peaks, one more peak O_{III} has been observed for the sample activated for 5, 10 and 30 minutes. The formation of this peak can be related to the presence of oxygen in oxygen deficient regions in ZnO host matrix, and is in accordance to the study of U. Ilyas et al. [18]

In order to study the vibrational properties of ZnO and to understand transport properties and phonon interaction with the free carriers we used Raman scattering. Also, to get the important information about the crystal structure, lattice distortion, phase transformation and defects [19]. Therefore, Raman spectroscopy techniques can be used to study the structural and morphological disorder, which are strongly correlated with optical phonons in nanostructures [20].

In the Raman spectra the non-polar E_2 (high) mode at ~ 438 cm^{-1} dominates, which originates from the first order scattering. This mode is primarily related to the vibrational motion of oxygen atoms in the ZnO crystal lattice. The intensity of these modes drastically decreases with the activation time. After 30 minutes of activation, E_2 (high) mode expands and increases its asymmetry towards lower frequencies, indicating a disorganization of the lattice and phonon - phonon interaction [21-23].

At initial non-activated powder, there is the presence of the first order mode, a weak polar mode A_1 (TO) at ~ 380 cm^{-1} and the presence of a very weak polar mode A_1 (LO) at about 568 cm^{-1}. Other modes derived from multiphonons process and among them the most intensive mode is the mode of the second order ~ 333 cm^{-1}. Activation of the powder leads to an increase in the intensity of A_1 (LO) mode. After 5 minutes of activation, we begin to observe the mode at 583 cm^{-1} which we can, according to Tzolov`s [24] and Wei`s [25] previous investigation, ascribe to first order mode E_1 (LO) and the position of the strongest mode of the second order A_1, (E_2(high) - E_2(low)) slightly shifted towards lower frequencies, from 333 cm^{-1} to 331 cm^{-1}. With the activation time an increasing in the A_1 (LO) + E_1 (LO) mode is observed. After activation of 10 min, this mode may indicate an increase in oxygen vacancies, because the increase of the concentration disrupts the long-range order in a grid, and thus leads to relaxation of Raman selection rules. Together with the peak at ~ 570-580 cm^{-1}, the increasing contribution of the Raman effect in the area of 545-555 cm^{-1} is observed, which is pronounced as a „shoulder" peak on the side of low frequency A_1 (LO) + E_1 (LO).

It is estimated that the activation time of 10 min or longer, this "shoulder" effect occurs as the result of two peaks. Thereby, the peak at ~ 545 cm^{-1}, according to literature [26, 27, 28] is associated with multiphonons process and the resulting contribution to the most convenient mode $2B_1$ low and 2LA in Γ, L, M, H point

Briluenove zone. The peak at 550-560 cm^{-1} may be caused by the vibration mode so called surface optical phonons, which is theoretically confirmed by Fonoberov and Baladin [29,30], and a defect may originate from the surface of the particles as well as the effects of the boundaries between the submicron domains.

With further activation, the mutual intensity ratio of the peaks A_1 (LO) + E_1 (LO) and E_2 (high) increase, which is caused by a significant reduction in the size of the powder particles. The increase in the peak intensities of A_1 (LO) + E_1 (LO) can be caused by so-called EFI (electric field induced) Raman amplification via the "charge trapping" at the grain boundaries, combined with coupled plasma-phonon scattering. The reason of that is because the grain boundaries of polycrystalline sample come up to a certain curvature energy gap (band banding) and to the presence of a relatively strong electric field [31]. The increase in the mentioned peak can also be caused by increased presence of surface phonons. Both effects are generally more pronounced in the case of small grain size, ie particles of powder and crystallite [24, 31], because in that case, the specific area of the observed polycrystalline sample increases. In support of the existence of the second effect is the observation that that aforementioned peak $2B_1$low mode and the existence of surface optical phonons becomes stronger and moves to 555 cm^{-1}, which may indicate an increased contribution of surface optical phonons, in relation to the activation of 10 min. This range looks like non-resonant spectrum of ZnO quantum dots ~ 20nm in diameter [32]. Particularly evident expansion of E_2 (high) mode and increase its asymmetry (toward lower frequencies) is arising from disorganization lattice and phonon-phonon interactions. Peak A_1 (LO) + E_1 (LO) is growing which confirms the existence of a peak $2B_1$ low. In the area of 700-2200 cm^{-1} the biggest changes occur. Modes in this range are highly amplified and the appearance of this part of the spectrum resembles the appearance of resonant amplification, although the line excitation at 633 nm (E = 1.96 eV), which is much less than the nominal band gap of ZnO (E = 3.3 eV).

In the range of 1140-1150 cm $^{-1}$ the dominant contribution, at about 1140-1150 cm^{-1} is derived from 2E1 (LO) mode in G point Briluenove zone, which belongs to the scattering of II order. Some authors, such as Cusco and associates [33], consider that in the area of 1150-1160 cm^{-1} there is a contribution 2A$_1$ (LO) mode (Overton A$_1$ (LO) mode) to G point Briluenove zones, and even that some contribution comes from 2LO scattering involving mixed mode the strip along the A-L-M line. In any case, there is agreement on the position that the Raman-effect of the 1140-1160 cm^{-1} does not include contributions of TO mode. Raman-effect, shows as a "shoulder" at around 1100 to 1110 cm^{-1} (Fig. 7) can be attributed to 2LO dispersed in the H and K counts Briluenove zone, while at about 1080 cm^{-1} can be note a smaller contribution of the A$_1$ (TO + LO). Otherwise, it is generally considered that the efficiency of Raman scattering is much higher for phonon processes involving LO mode, than processes involving TO mode. For example, Calleja and Cardona [26] reported that 2LO resonant scattering can be increased for the photon energy around ~ 1eV under basic energy zone. The fact that in the mechanically activated powder practically there was no change in the intensity of A$_1$ (TO) mode (except for a slight weakening in the activation of the 5 min) and a significant gain of LO mode, supports the assumption of the occurrence of resonance amplification in the powders activated for 30 min. The Callender et al [34] in the case of ZnO single crystals found that this mode does not depend on the wavelength of the excitation laser radiation, while the intensity E$_1$ (LO) mode increases significantly if there is the conditions for resonant amplification, and this coincides with what was observed in our research Powdered activated for 30 min.

This could indicate that the resonant amplification occurs through the levels in the forbidden zone [31]. Also, the appearance of the 3LO mode, i.e. the scattering of the third order in the sample ZnO - 30min further shows the Raman resonance dispersion [31, 35]. It is a resonant amplification across levels in the energy gap [23, 33], which in this case is referred to the intermediate electronic states of defects created during mechanical activation.

When measuring in the range of above 20 cm^{-1} (third extended measurement) with the ZnO -activated for 30 minutes the phenomena E_2 (low) non-polar first order mode at 98cm^{-1} is observed and binds the vibration zinc sublattice (Fig. 6.) [23,33]. It is observed that the modes E_2 (low) of greater intensity than the E_2 (high), which is usually the case for non-resonant scattering. To verify the above mentioned results, additional measurements were done with two more laser wavelengths, one at 442 nm and the other at 785 nm.

The Figs. 9. and 10. show that the laser excitation of 785 nm appears as a typical spectrum of non-resonant scattering. In the range of 20 cm^{-1} to 800 cm^{-1} the most intense peak is E_2(low) then E_2(high). The influence of Raman effect at ~ 545-560 cm^{-1}, can be notice as a shoulder at A_1 (LO) + E_1 (LO) peak that originate from surface optical phonons. The most intensive E_2 (low) mode is related to the vibration of the zinc sublattice [21, 23]. The intensity of the E_2 (low) mode is stronger than the intensity of E_2 (high) mode and this is a typical case of non-resonant scattering.

Raman spectrum of the ZnO-30 sample is obtained at the laser excitation wavelength of 442 nm and looks like the resonance Raman scattering spectrum. In the range of 20 cm^{-1} to 2200cm^{-1} (Fig. 9.) the most intense peak is A_1 (LO) + E_1 (LO) mode at 573 cm^{-1} and 578cm^{-1}, which is due to resonant scattering, because of which and peak at ~ 1168cm^{-1} derived from the mode 2E_1 (LO) is highlighted. With activation time up to 10 minutes “blue shift” of peak A_1 (LO) + E_1 (LO) for more than 10 cm^{-1}, while after 30 minutes of activation peak goes left toward lower frequencies than non activated powder. E_2 (high) mode is getting lower whit activation time and after 30 minutes of activation the ratio of peaks E_2 (high) and A_1 (LO) + E_1 (LO) is equal to 1:4. E_2 (high) mode shifts to higher frequencies with activation time of 5 and 10 minutes. The above mentioned peak for powder activated for 30 minutes takes the position at a lower frequency than the non-activated powder. This is in accordance with the crystallite size (~ 30 nm) calculated by the Rietveld’s method [22] . Blue shift of the E_2 (high) mode can be observed as extensive increase of compression type strain, concentration of defects increases which leads to the localization of phonons by defects inherent in the structure of ZnO, such as oxygen vacancies and Zn interstitial, resulting in the E_2 (high) mode and A_1 (LO) + E_1 (LO) peak shifted to the left compared to the other powders. In addition, the longest activation results in the significantly reduced size of the crystallites and changes in the dominant type of stress in terms of domination of stress-type strain, and possibly a change in the dominant type of defects, which also leads to a shift to lower-mentioned mode frequencies.

4. Conclusion

In this article the results of structural investigation of mechanically activated ZnO powders have been presented. It was noticed that mechanical activation caused the increase of mesopore volume and non-monotonic trends of specific surface area with prolonged milling time. These effects are caused by powder particle adhesion and breakage due mechanical activation. TEM images showed erosion of the surface as well as diminution of the particles and the formation of agglomerates for powder activated for 30 minutes. SEM micrographs are in accordance with TEM analysis, also increase of surface agglomeration to approximately 1 micron is noticed. Microstructure analysis showed Results obtained by Rietveld method show a significant decrease in the crystallite size from ~65 to 35nm and increase in the microstain up to 1,2%. Obtained results report the creation of defect and increase of strain inside the hexagonal lattice of ZnO powder for prolonged time of mechanical activation. For the mechanically activated samples it was noticed that the main core level XPS spectrum of Zn 2p is slightly asymmetrical. This is indicating the existence of Zn in its multiple-oxidation states. The lower energy peak in the deconvoluted spectrum is attributed to the Zn^{2+} ion array surrounded by O^{2-} ions in the hexagonal ZnO, while the deconvoluted peak centered at the higher binding energy side is related to metallic zinc. For O1s, beside two peaks (O_I and O_{II}) for non-activated powder, one more peak O_{III} has been observed for the sample activated for 5, 10 and 30 minutes. The formation of this peak can be related to the presence of oxygen in oxygen deficient regions in ZnO host matrix. Investigation of Raman spectra showed the “blue shift” of Raman E_2(high) mode and it lose it intensity, with activation time, as a consequence of the compression type of stress.

Unexpected “red shift” of the same Raman mode, for powder activated for the longest time, showed the intrinsic defect formation combined with confinement size effect. For the same sample it is also noticed interesting resonant Raman scattering in the range of

700-2000 cm^{-1} for initial laser wavelength of 633 nm. Obtained results indicate that mechanical activation introduced the enhancement over the levels in the gap which in our case would represent defects created during mechanical activation. In order to verify above mentioned resonant Raman scattering we applied two different laser wavelength 442 nm and 785nm. Measurements at 442 nm confirmed “red shift” of E_2 (high) mode for powder activated for 30 minutes. Also it was noticed a significant shifts (10-20 cm^{-1}) of a large number of Raman mode due to activation time by laser-induced heating. The results of the non-resonant Raman scattering obtained at 785 nm are opposite of the Raman scattering at the 442 nm. This type of changes should be more investigated.

Acknowledgement

This research was performed within the projects OI 172057 financed by the Ministry of Education, Science and Technological Development of the Republic of Serbia and NSF CREST (HRD-0833184), NASA (NNX09AV07A) and Project F/198, funded by the Serbian Academy of Science and Arts.

References

[1] C. P. Fah, J. Xue, J. Wang, Nanosized Zinc-Oxide Particles Derived from Mechanical Activation of $Zn_5(NO_3)_2(OH)_8{\cdot}2H_2O$ in Sodium Chloride, J. Am. Ceram. Soc., 85 (2002) 273–75

[2] M. Šćepanović, M. Grujić-Brojčin, K. Vojisavljević, T. Srećković, Defect induced variation in vibrational and optoelectronic properties of mamocrystaline ZnO powders, J. Appl. Phys. 109 (2011) 034313-1-8

[3] J. Huang, Y. Wu, C. Gu, M. Zhai, Y. Sun, J. Liu, Fabrication and gas-sensing properties of hierarchically porous ZnO architectures, Sensor Actuat. B 155 (2011) 126–133

[4] A. Stanković, Z. Stojanović, Lj. Veselinović, S. D. Škapin, S. Marković, D. Uskoković, ZnO micro and nanocrysrals with enhanced visibe light absorption Mat. Sci. Eng. B 177 (2012) 1038-1045

[5] Z. Zang, A. Nakamura, J. Temmyo, Single cuprous oxide films synthesized by radical oxidation at low temperature for PV application, Optics Express, Vol. 21, Issue 9, pp. 11448-11456 (2013).

[6] Z. Zang, A. Nakamura, J. Temmyo, Nitrogen doping in cuprous oxide films synthesized by radical oxidation at low temperature, Mater Lett 2013;92:188-191.

[7] C. P. Fah, J. Wang, Effect of high-energy mechanical activation on the microstructure and electrical properties of ZnO-based varistors, Solid State Ionics 132 (2000) 107–117

[8] V. Ischenko, S. Polarz, D. Grote, V. Stavarache, K. Fink and M. Driess, Zinc Oxide Nanoparticles with Defect, Adv. Funct. Mater. 15 (1954) 1945–1954

[9] N. Nikolić, T. Srecćković, M.M. Ristić, The influence of mechanical activation on zinc stannate spinel formation, J. Eur. Ceram. Soc. 21 (2001) 2071–2074

[10] M. Šćepanović, T. Srećković, K. Vojisavljević, M. M. Ristić, Modification of the Structural and Optical Properties of Commercial ZnO Powder by Mechanical Activation, Sci. Sint., 38 (2006) 169-175

[11] , M. M Ristić, and S. Dj. Milošević, Mechanical Activation of Inorganic Materials, Serbian Academy of Sciences and Arts, Belgrade, 1998

[12] N Hasuike, H Fukumura, H Harima, K Kisoda, H Matsui, H Saeki, and H Tabata, Raman scattering studies on ZnO doped with Ga andN (codoping), and magnetic impurities, J. Phys.: Condens. Matter. 16 (2004) S5807–S5810

[13] V.P. Pavlović, J. Krstić, M.J. Šćepanović, J. Dojčilović, D. M. Minić, J. Blanuša, S. Stevanović, V. Mitić, V. B. Pavlović, Structural investigation of mechanically activated nanocrystalline $BaTiO_3$ powders., Ceram. Inter. 37 (2011) 2513-2518

[14] H. Ferkel and R.J. Hellmig ,Effect Of Nanopowder Deagglomeration On The Densities Of Nanocrystalline Ceramic Green Bodies And Their Sintering Behaviour, NanoStructured Materials, Vol. 11, No. 5, pp. 617–622, 1999]

[15] R. Cheary, A. Coelho, A Fundamental Parameters Approach to X-ray Line-Profile Fitting, J. Appl. Cryst. (1992) 25,109-121

[16] U.Ilyas, P. Lee and T. L. Tan, R. V. Ramanujan, R. Chen and H. D. Sun, R. S. Rawat, High temperature ferromagnetic ordering in c-axis oriented ZnO:Mn nanoparticle thin films by tailoring substrate temperature Plasma Science and Applications, International Journal of Modern Physics: Conference Series Vol. 32 (2014), 1460341

[17] Y. Y. Chen, J. C. Hsu, C. Y. Lee and P. W. Wang, Journal of Material Science 48, 1225 (2013).

[18] U. Ilyas, R. S. Rawat, G. Roshan, T. L. Tan, P. Lee, S. V. Springham, S. Zhang, L. Fengji, R. Chen and H. D. Sun, Appl. Surf. Sci. 258, 890 (2011).

[19] Y. Huang, M. Liu, Z. Li, Y. Zeng, S. Liu, Raman spectroscopy study of ZnO-based ceramic films fabricated by novel sol-gel process, Mat. Sci. Eng. B 97 (2003) 111-116

[20] M. Scepanovic, M. Grujic-Brojcin, K. Vojisavljevic S. Bernik and T. Sreckovic, Raman study of structural disorder in ZnO nanopowders, J. Raman Spectrosc. 2010, 41, 914–921

[21] K.-F. Lin, H.-M. Cheng, H.-C. Hsu, W.-F. Hsieh, Size dependence of photoluminescence and resonant Raman scattering from ZnO quantum dots, Appl. Phys. Lett. 88 **(**2006) 263117-1-3

[22] I. Calizo, K. A. Alim, V. A. Fonoberov, S. Krishnakumar, M. Shamsa, A. A. Balandin, R. Kurtz, Micro-Raman spectroscopic characterization of ZnO quantum dots, nanocrystals and nanowires, Proc. of SPIE 6481 (2007) 64810N-1-8

[23] S. Samuel, J. Koshy, A. Chandran, K. C. George, Optical phonon confinement in ZnO nanorods and nanotubes Indian J. Pure & Appl. Phys. 48 (2010) 703-708

[24] M. Tzolov, N. Tzenov, D. Dimova-Malinovska, M. Kalitzova, C. Pizzuto, G. Vitali, G. Zollo, I. Ivanov,Vibrational properties and structure of undoped and Al-doped ZnO films deposited by RF magnetron sputtering, Thin Solid Films 379 (2000) 28-36

[25] X. Q. Wei, B. Y. Man, M. Liu, C. S. Xue, H. Z. Zhuang, C. Yang, Blue luminescent centers and microstructural evaluation by XPS and Raman in ZnO thin films annealed in vacuum, N_2 and O_2, Physica B 388 (2007) 145–152

[26] J. M. Calleja, M. Cardona Resonant Raman scattering in ZnO, Phys. Rev. B 16 (1977) 3753-3761

[27] R. Sanz, J.Jensen, G.Gonzalez-Diaz, O.Martinez, M.Vazquez, M. Hernandez-Velez, Continuous and localized Mn implantation of ZnO, Nanoscale Res. Lett. 4 (2009) 878-887

[28] B. H. Soni, M. P. Deshpande, S. V. Bhatt, S. H. Chaki, V. Sathe, X-ray diffraction, X-ray photoelectron spectroscopy, and raman spectroscopy of undoped and Mn-doped ZnO nanoparticles prepared by microwave irradiation, J. Appl. Spectros., 79 (2013) 901-907

[29] V. A. Fonoberov and A. A. Balandin, Interface and confined optical phonons in wurtzite nanocrystals, Phys. Rev. B 70, (2004) 233205

[30] V. A. Fonoberov and A. Balandin, Polar optical phonons in wurtzite spheroidal quantum dots: theory and application to ZnO and ZnO/MgZnO nanostructures, J. Phys.: Condens. Matter 17, (2005) 1085

[31] Roy, S. Byrne, E. McGlynn, J-P Mosnier, E. de Posada, D. O’Mahony, J. G. Lunney, M. Henry, B. Ryan, A.A. Cafolla,Correlation of Raman and X-ray diffraction measurements of annealed pulsed laser deposited ZnO thin films, Thin Solid Films 436 (2003) 273-276

[32] K.A. Alim, V.A. Fonoberov, A. A. Balandin, Appl. Phys. Lett. 86 (2005) 053103-1-3C.

[33] R. Cuscó, E. A. Lladó, J. Ibáñez, L. Artús, J. Jiménez, B. Wang, M. J. Callahan, Temperature dependence of Raman scattering in ZnO, Phys. Rev. B 75 (2007) 165202-1-11

[34] R. H. Callender, S. S. Sussman, M. Selders, and R. K. Chang, Dispersion of Raman Cross Section in CdS and ZnO over a Wide Energy Range, Phys. Rev. B 7 (1973), 3788

[35] F. Friedrich, N. H. Nickel, Resonant Raman scattering in hydrogen and nitrogen doped ZnO, Appl. Phys. Lett.91, (2007) 111903-1-3

Fig. 1. Mesopore volume and specific surface area as a function of activation time.

Fig. 2. TEM images of ZnO powder: a) nonactivated, , b) activated for 5 minutes, c) activated for 10 minutes and d) activated for 30 minutes.

Fig. 3. SEM micrographs of ZnO powder: a) nonactivated, b) activated for 5 minutes, c) activated for 10 minutes and d) activated for 30 minutes.

Fig. 4. XRD patterns of ZnO powders.

Fig. 5. Changes in crystallite size with activation time.

Fig. 6. XPS spectra of ZnO powders, a) Zn2p and b) O1s

Fig. 7. Raman spectra of ZnO powders obtained with laser wavelength of 633nm (The first and second measurement in the range above 200 cm^{-1}).

Fig. 8. Comparative graph of three different measurements of ZnO activated for 30 minutes.

Fig. 9. Comparative graph of measurement with three different laser excitation in a range of 20-800 cm^{-1}.

Fig. 10. Comparative graph of measurement with three different laser excitation in a range of 200-2200 cm^{-1}.

Table 1 Particle size of ZnO powders obtained by SEM micrographs

Activation time, (min)	**Particle size, (nm)**
0	212-704
5	98-545
10	76-510
30	64-464

Table 2 Lattice parameters and unite cell volume.

Activation time, (min)	**a (Å)**	**c (Å)**	**v (Å^3)**
0	3.25059	5.20783	47.67
5	3.25053	5.20802	47.66
10	3.25143	5.20935	47.69

30	3.25177	5.20926	47.70

Fig1.

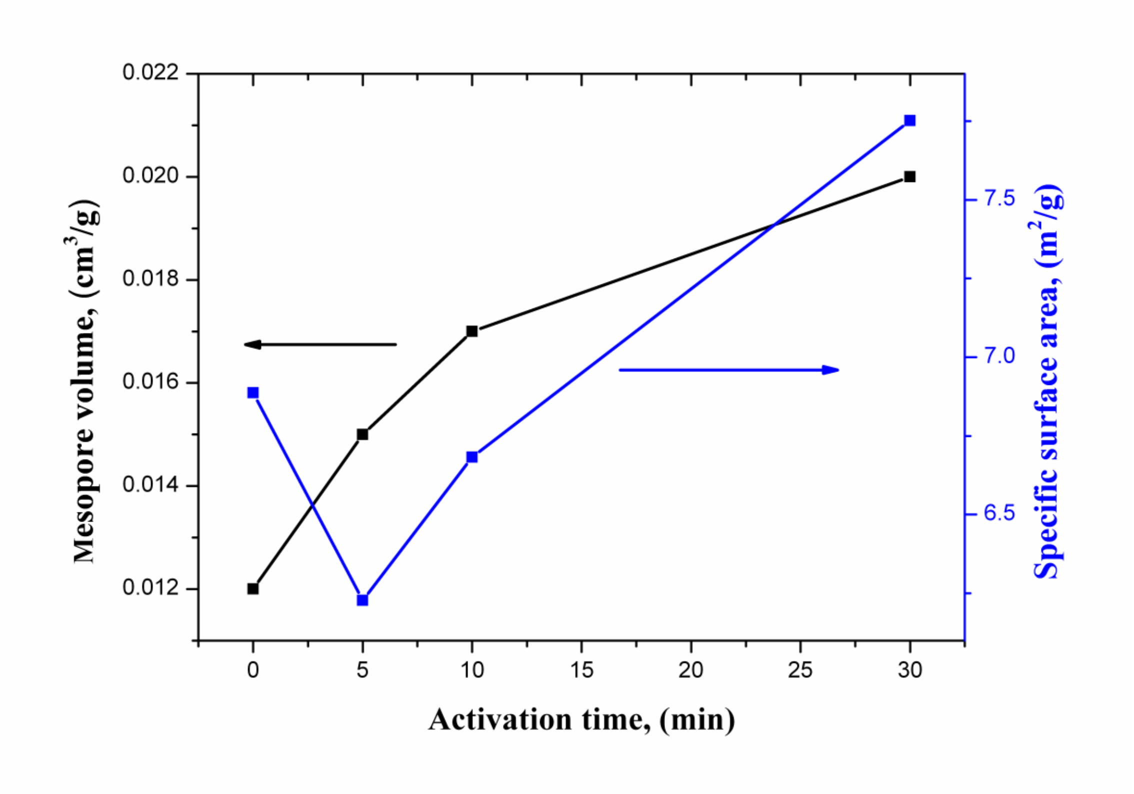

Fig. 2a

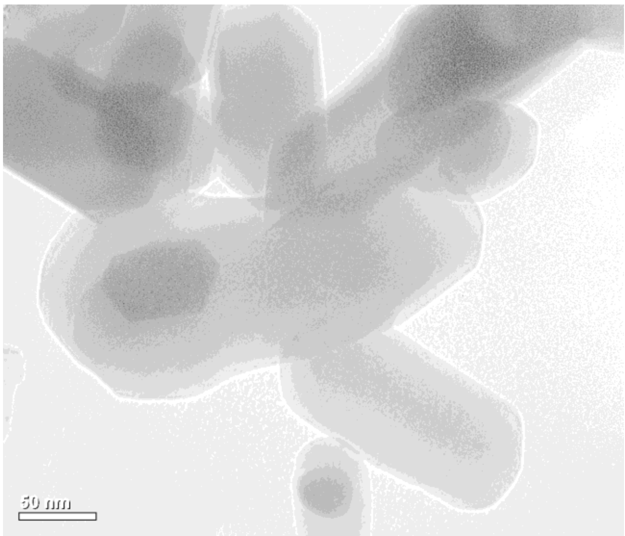

Fig. 2b

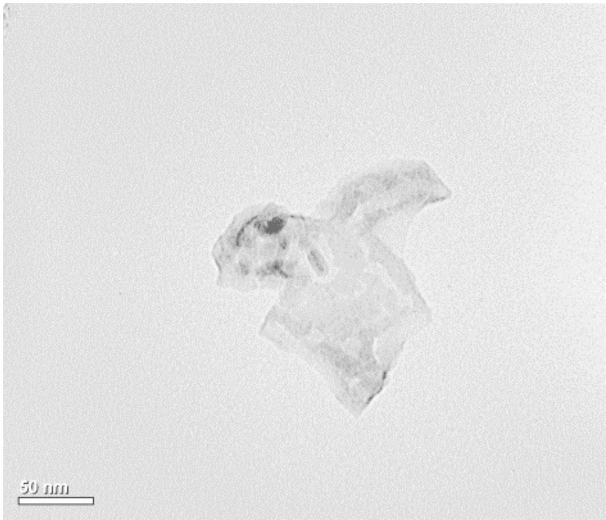

Fig.2c

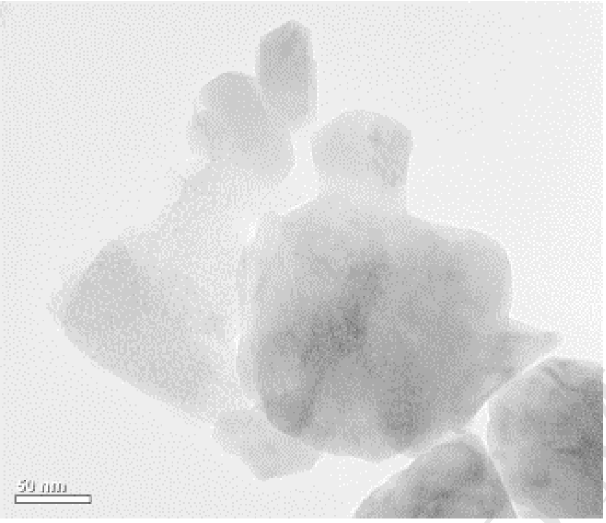

Fig. 2d

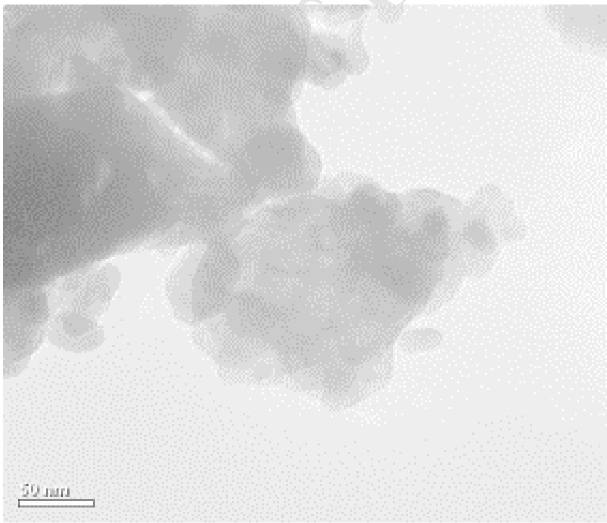

Fig. 3 a

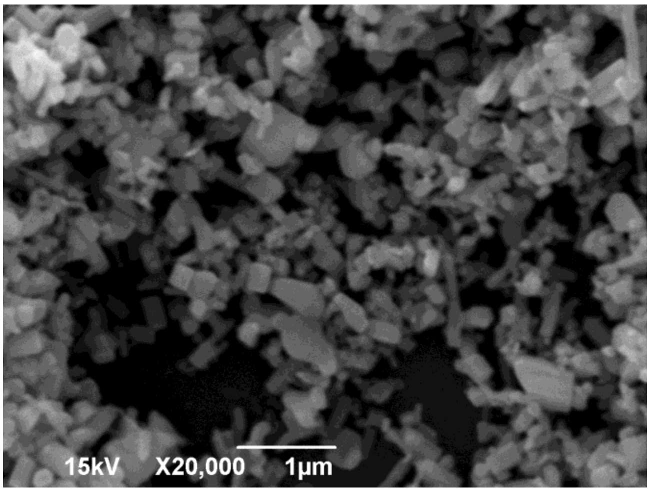
15kV
X20,000
1µm

Fig. 3b

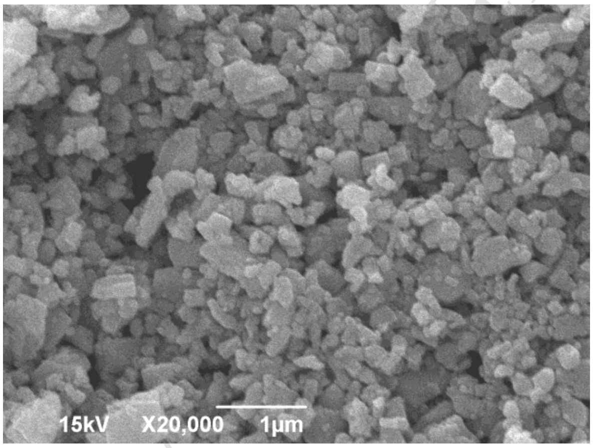
15kV
X20,000
1µm

Fig. 3c

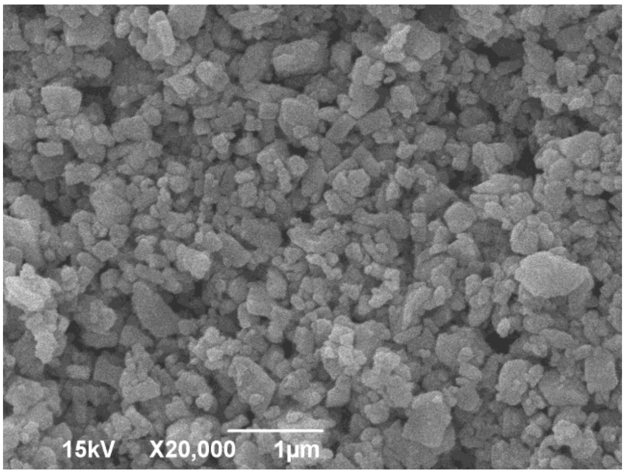
15kV X20,000 1μm

Fig. 3d

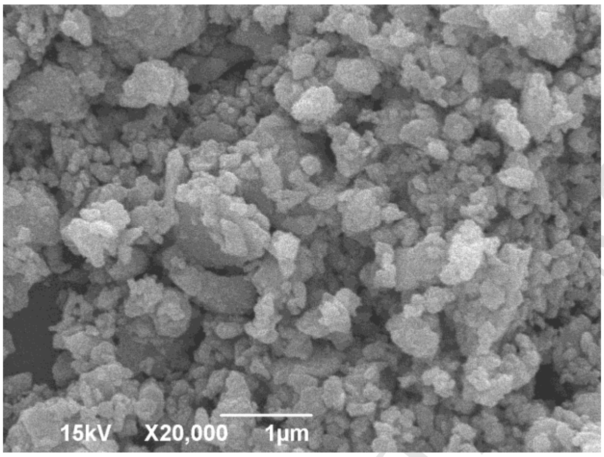
15kV X20,000 1μm

Fig.4.

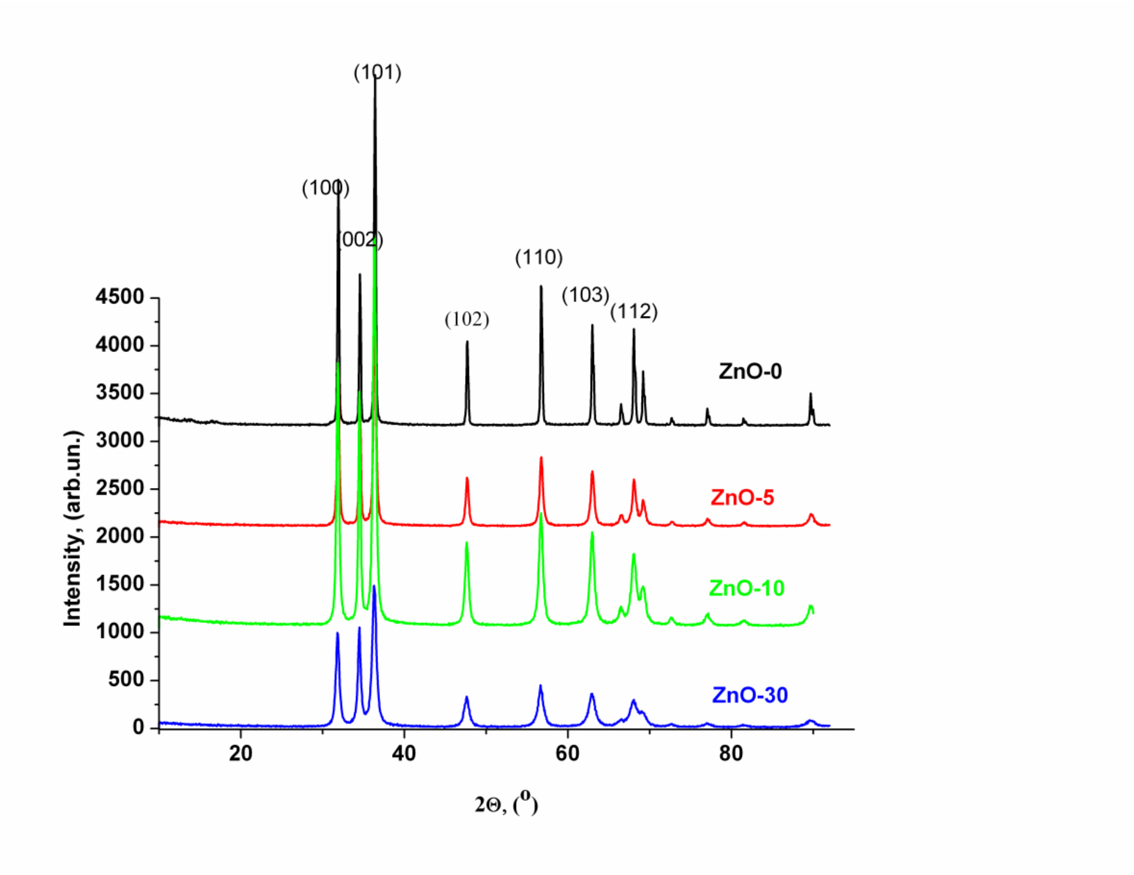
(101)
(100)
(002)
(110)
(103)
(112)
(102)
ZnO-0
ZnO-5
ZnO-10
ZnO-30
Intensity, (arb.un.)
4500
4000
3500
3000
2500
2000
1500
1000
500
0
20
40
60
80
2Θ, (°)

Fig. 5

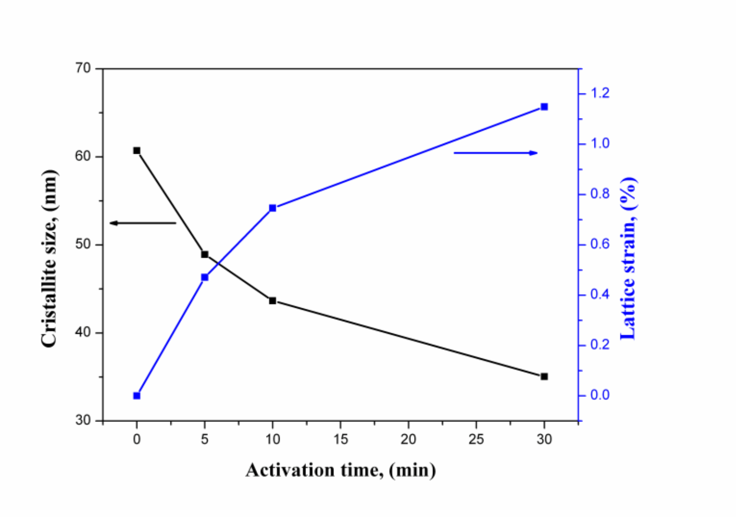
Cristallite size, (nm)
70
60
50
40
30
Lattice strain, (%)
1.2
1.0
0.8
0.6
0.4
0.2
0.0
0
5
10
15
20
25
30
Activation time, (min)

Fig. 6a)

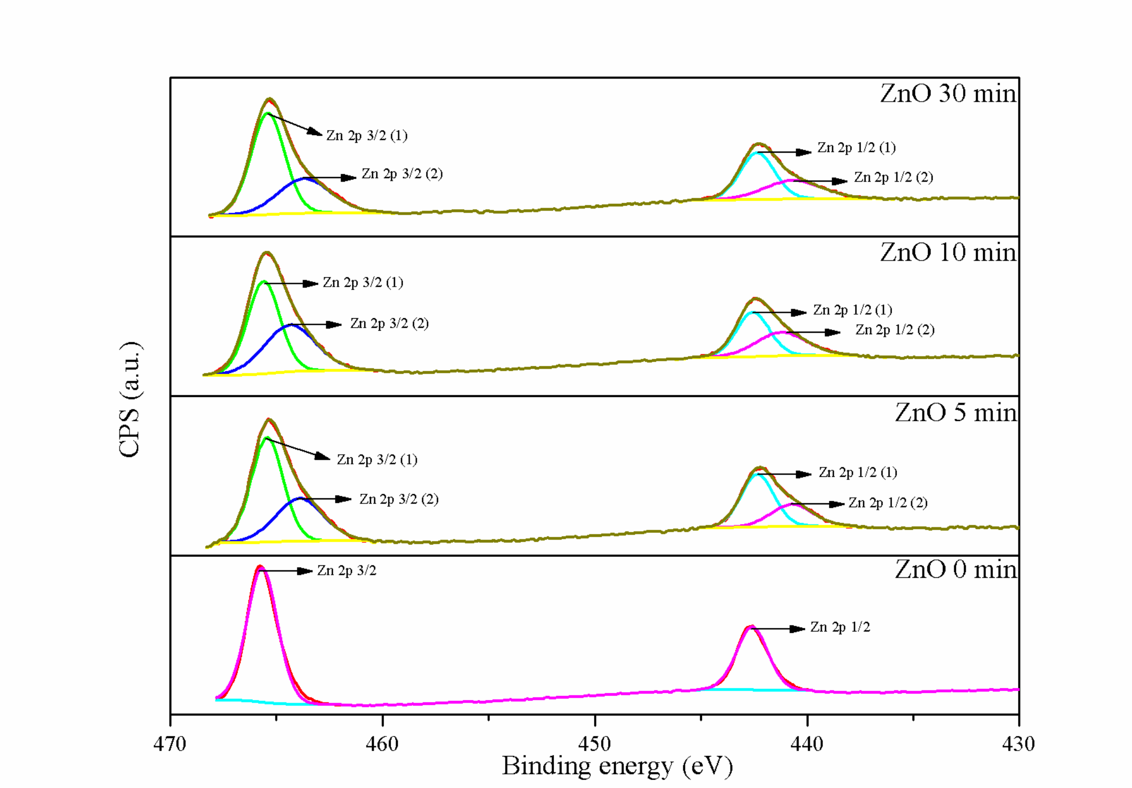
ZnO 30 min
Zn 2p 3/2 (1)
Zn 2p 3/2 (2)
Zn 2p 1/2 (1)
Zn 2p 1/2 (2)
ZnO 10 min
Zn 2p 3/2 (1)
Zn 2p 3/2 (2)
Zn 2p 1/2 (1)
Zn 2p 1/2 (2)
ZnO 5 min
Zn 2p 3/2 (1)
Zn 2p 3/2 (2)
Zn 2p 1/2 (1)
Zn 2p 1/2 (2)
ZnO 0 min
Zn 2p 3/2
Zn 2p 1/2
CPS (a.u.)
470
460
450
440
430
Binding energy (eV)

Fig. 6b)

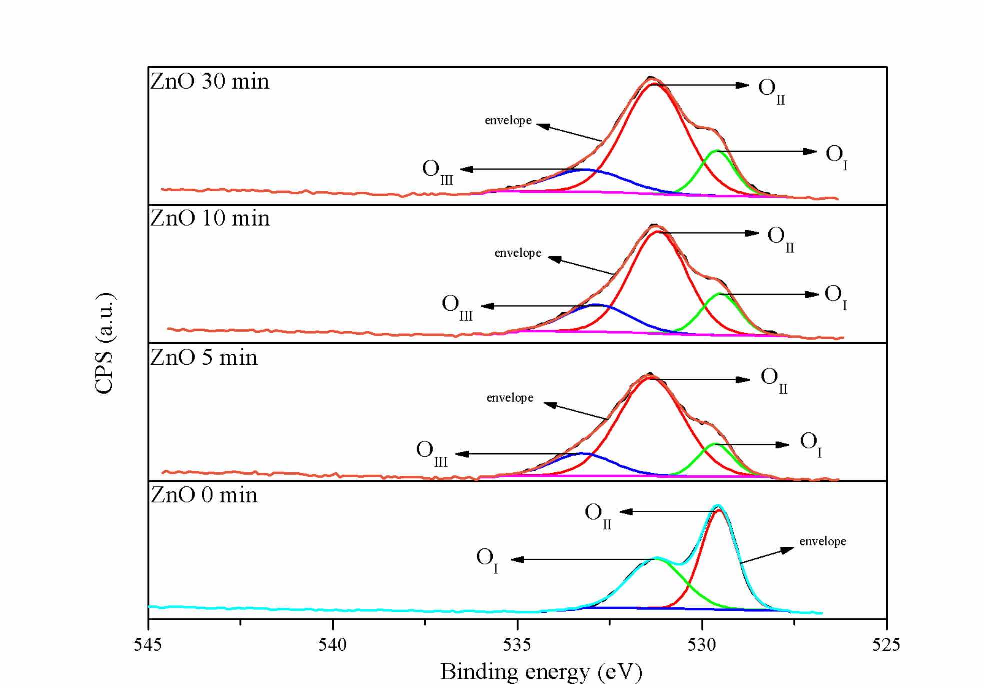
ZnO 30 min
O_II
envelope
O_I
O_III
ZnO 10 min
O_II
envelope
O_III
O_I
ZnO 5 min
O_II
envelope
O_III
O_I
ZnO 0 min
O_II
O_I
envelope
CPS (a.u.)
545
540
535
530
525
Binding energy (eV)

Fig. 7

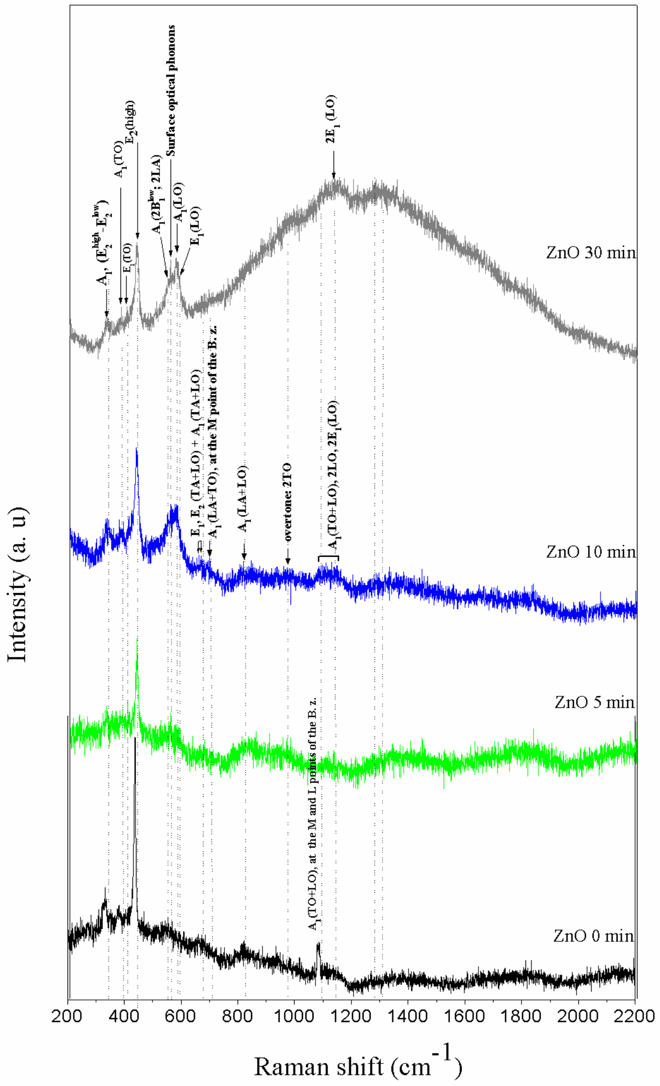
A1, (E2high-E2low)
E1(TO)
A1(TO)
E2(high)
A1(2B1low; 2LA)
Surface optical phonons
A1(LO)
E1(LO)
2E1 (LO)
E1, E2 (TA+LO) + A1(TA+LO)
A1(LA+TO), at the M point of the B. z.
A1(LA+LO)
overtone 2TO
A1(TO+LO), 2LO, 2E1(LO)
A1(TO+LO), at the M and L points of the B. z.
ZnO 30 min
ZnO 10 min
ZnO 5 min
ZnO 0 min
Intensity (a. u)
Raman shift (cm-1)
200
400
600
800
1000
1200
1400
1600
1800
2000
2200

Fig. 8

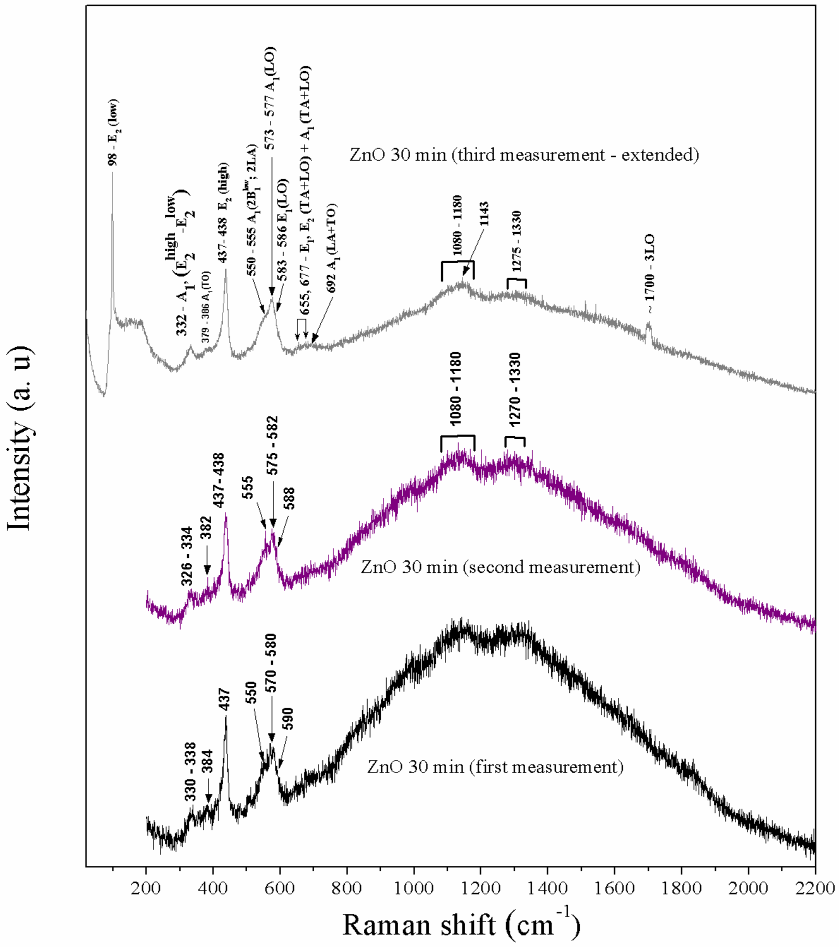

ACCEPTED

Fig. 9

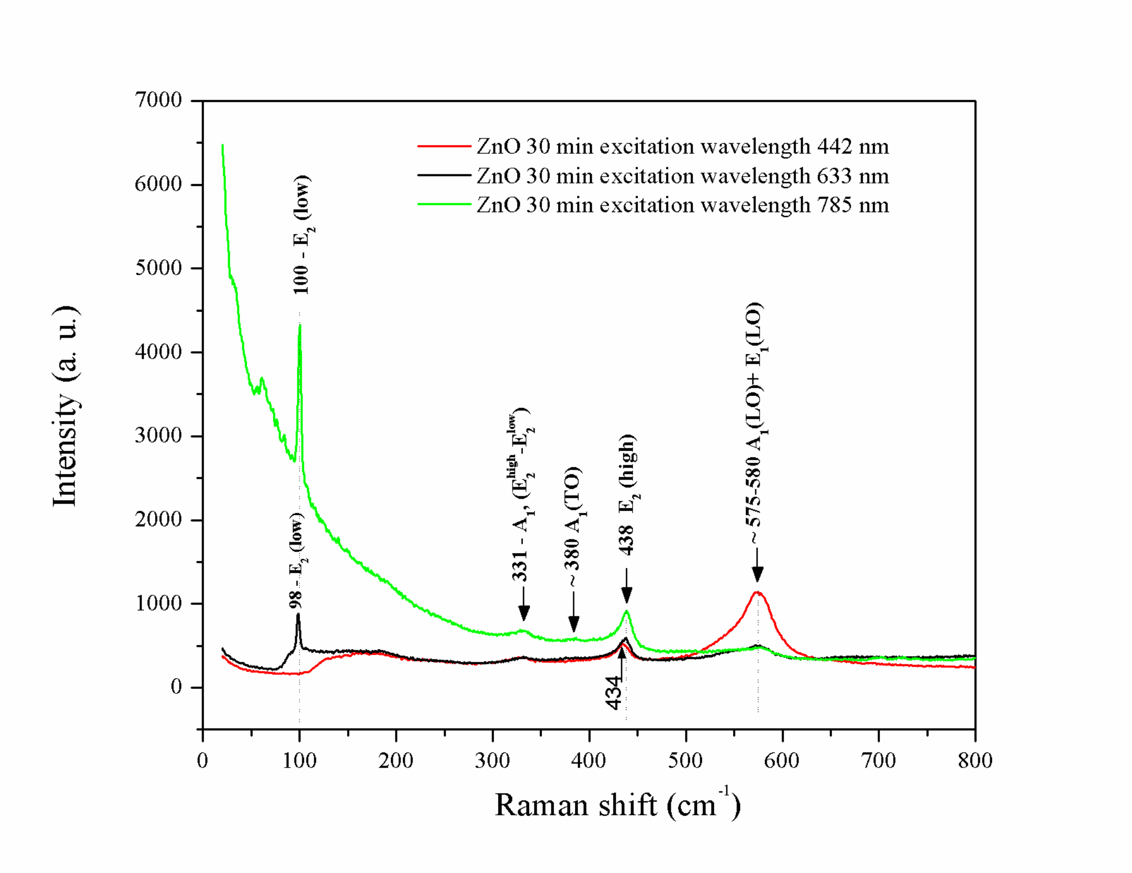

ACCEPTED

Fig. 10.

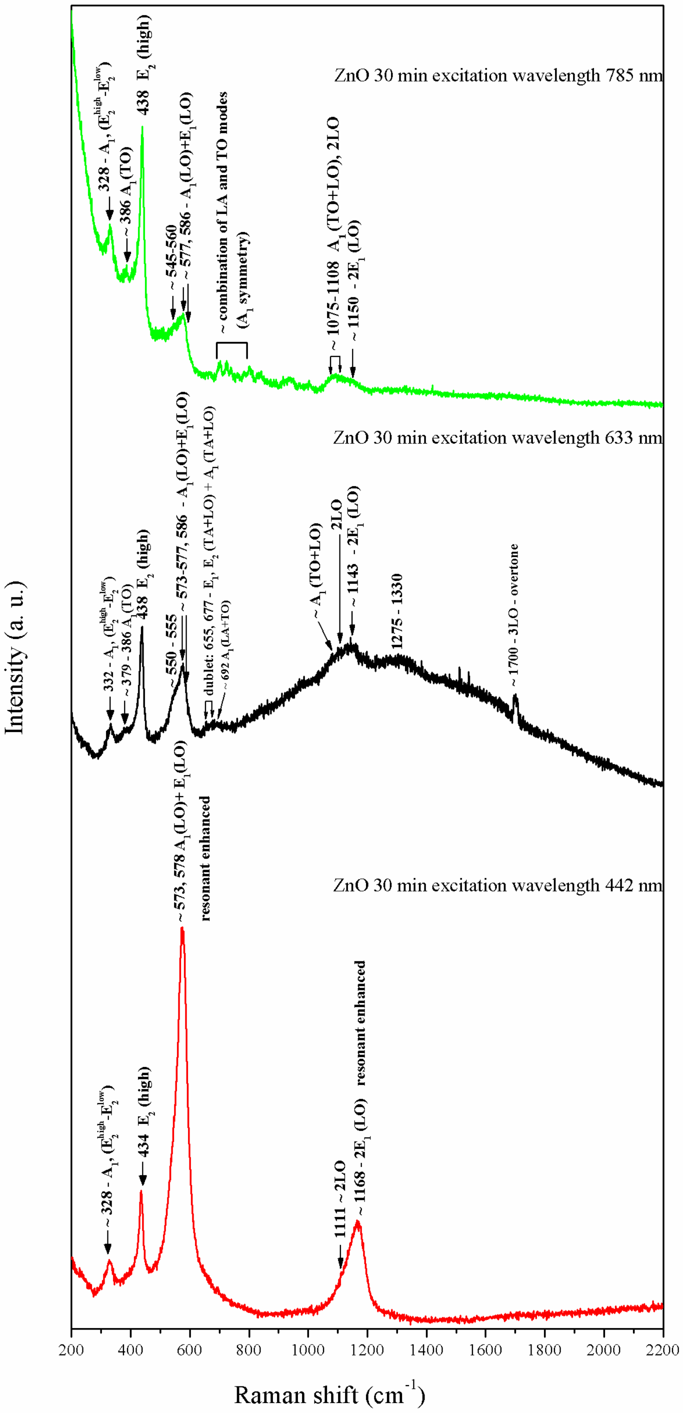
ZnO 30 min excitation wavelength 785 nm
328 - A$_1$, (E$_2^{high}$-E$_2^{low}$)
~ 386 A$_1$(TO)
438 E$_2$ (high)
~ 545-560
~ 577, 586 - A$_1$(LO)+E$_1$(LO)
~ combination of LA and TO modes (A$_1$ symmetry)
~ 1075-1108 A$_1$(TO+LO), 2LO
~ 1150 - 2E$_1$ (LO)
ZnO 30 min excitation wavelength 633 nm
332 - A$_1$, (E$_2^{high}$-E$_2^{low}$)
~ 379 - 386 A$_1$(TO)
438 E$_2$ (high)
~ 550 - 555
~ 573-577, 586 - A$_1$(LO)+E$_1$(LO)
dublet: 655, 677 - E$_1$, E$_2$ (TA+LO) + A$_1$ (TA+LO)
~ 692 A$_1$(LA+TO)
~ A$_1$ (TO+LO)
2LO
~ 1143 - 2E$_1$ (LO)
1275 - 1330
~ 1700 - 3LO - overtone
ZnO 30 min excitation wavelength 442 nm
~ 328 - A$_1$, (E$_2^{high}$-E$_2^{low}$)
434 E$_2$ (high)
~ 573, 578 A$_1$(LO)+ E$_1$(LO)
resonant enhanced
1111 ~2LO
~ 1168 - 2E$_1$ (LO) resonant enhanced
Intensity (a. u.)
200
400
600
800
1000
1200
1400
1600
1800
2000
2200
Raman shift (cm^{-1})

In this article, the authors investigated the structural characteristics of mechanically activated ZnO powder. Results obtained by Rietveld method show a significant decrease in the crystallite size from ~65 to 35nm and increase in the microstain up to 1,2%. Obtained results report the creation of defect and increase of strain inside the hexagonal lattice of ZnO powder for prolonged time of mechanical activation. Raman spectra results indicate that mechanical activation introduced the enhancement over the levels in the gap which in our case would represent defects created during mechanical activation. Fig. 6a) and Fig. 6b) shows the XPS diagrams. For the mechanically activated samples it was noticed that the main core level XPS spectrum of Zn 2p is slightly asymmetrical, indicating the existence of Zn in its multiple-oxidation states. For O1s, beside two peaks (O_I and O_{II}) for non-activated powder, one more peak O_{III} has been observed for the sample activated for 5, 10 and 30 minutes. The formation of this peak can be related to the presence of oxygen in oxygen deficient regions in ZnO host matrix.

Fig. 6a)

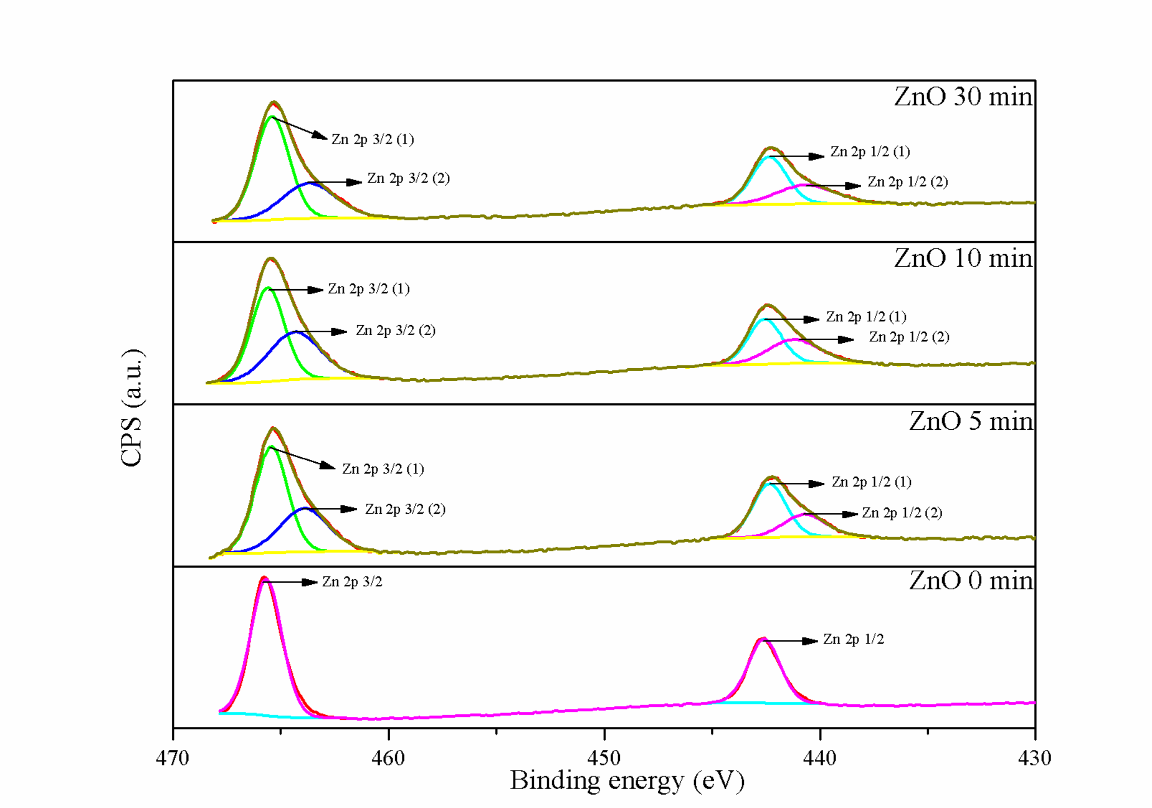

Fig. 6b)

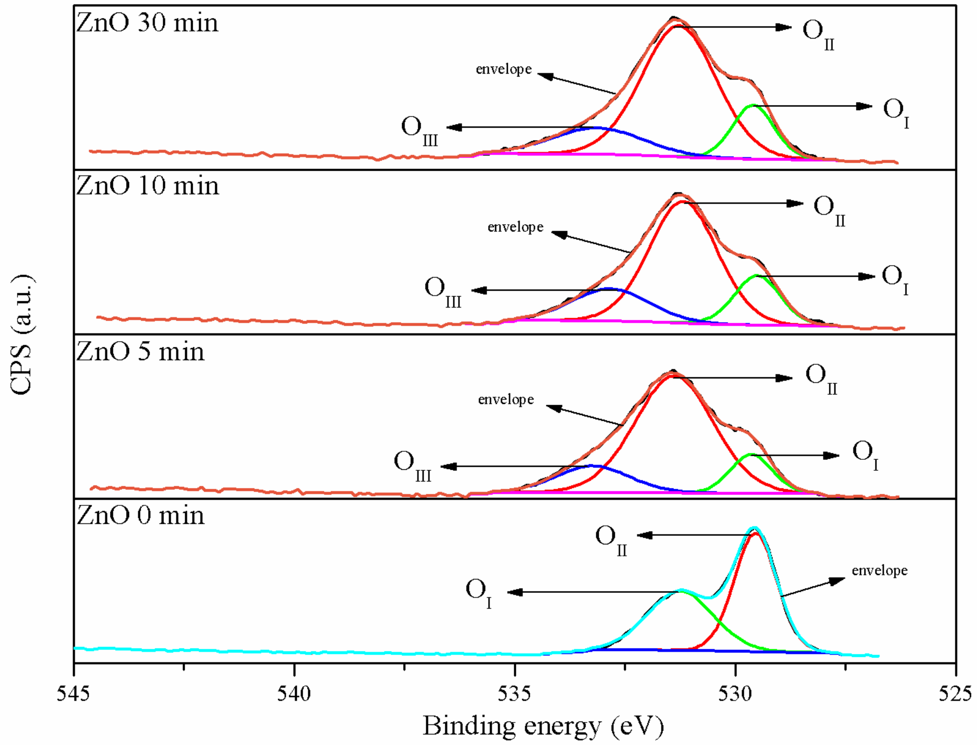

Fig 6. XPS spectra of ZnO powders, a) Zn2p and b) O1s

*Highlights (for review)

Structural characteristics of mechanically activated ZnO powder were investigated. The peak intensities are getting lower and expend with activation time. In Raman spectra some changes along with atypical resonant scattering were noticed.

Fig. 1. Mesopore volume and specific surface area as a function of activation time.

Fig. 2. TEM images of ZnO powder: a) nonactivated, , b) activated for 5 minutes, c) activated for 10 minutes and d) activated for 30 minutes.

Fig. 3. SEM micrographs of ZnO powder: a) nonactivated, b) activated for 5 minutes, c) activated for 10 minutes and d) activated for 30 minutes.

Fig. 4. XRD patterns of ZnO powders.

Fig. 5. Changes in crystallite size with activation time.

Fig. 6. XPS spectra of ZnO powders, a) Zn2p and b) O1s

Fig. 7. Raman spectra of ZnO powders obtained with laser wavelength of 633nm (The first and second measurement in the range above 200 cm^{-1}).

Fig. 8. Comparative graph of three different measurements of ZnO activated for 30 minutes.

Fig. 9. Comparative graph of measurement with three different laser excitation in a range of 20-800 cm^{-1}.

Fig. 10. Comparative graph of measurement with three different laser excitation in a range of 200-2200 cm^{-1}.

Fig.1

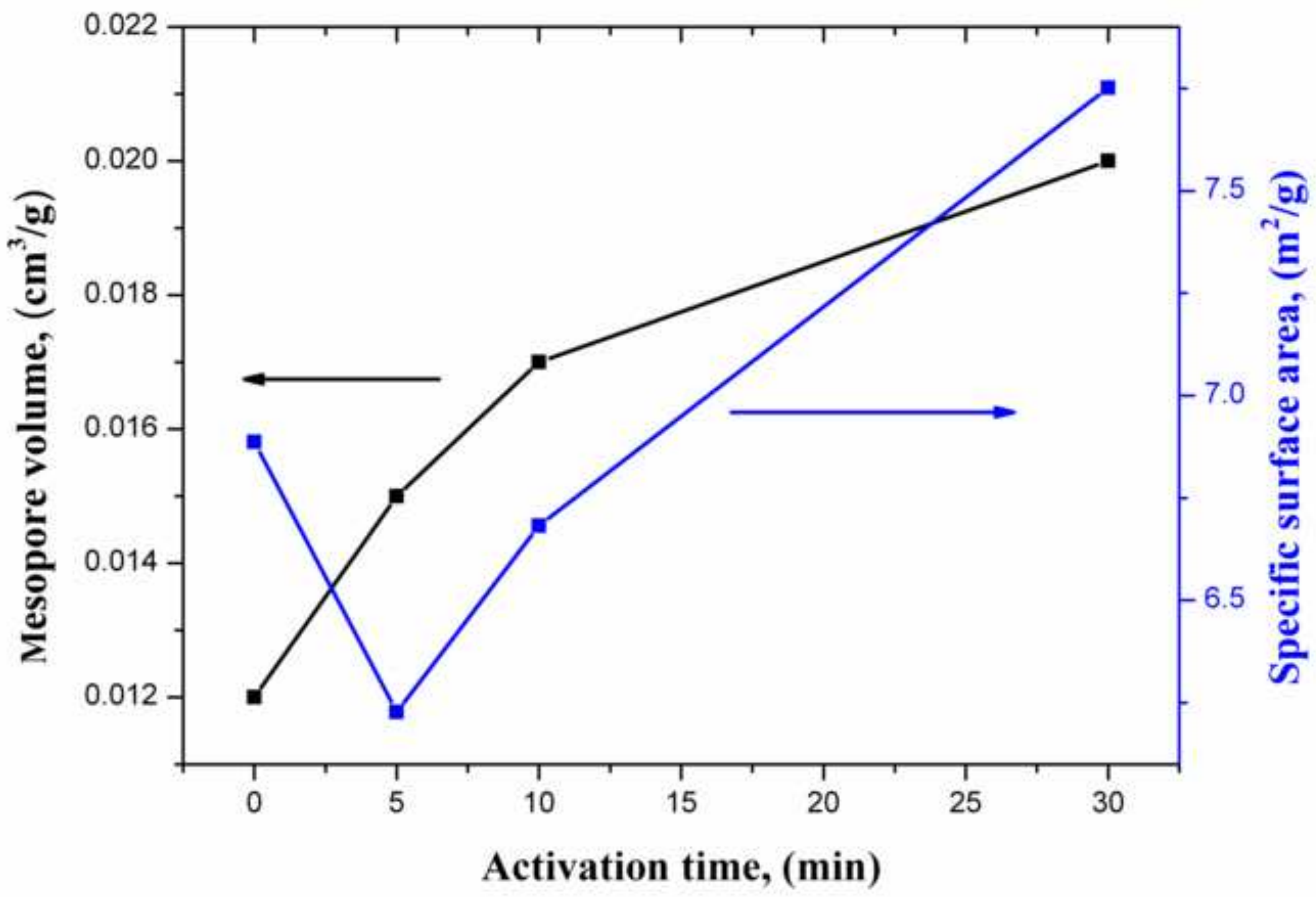
0.022
0.020
0.018
0.016
0.014
0.012
Mesopore volume, (cm³/g)
7.5
7.0
6.5
Specific surface area, (m²/g)
0
5
10
15
20
25
30
Activation time, (min)

Fig. 2a

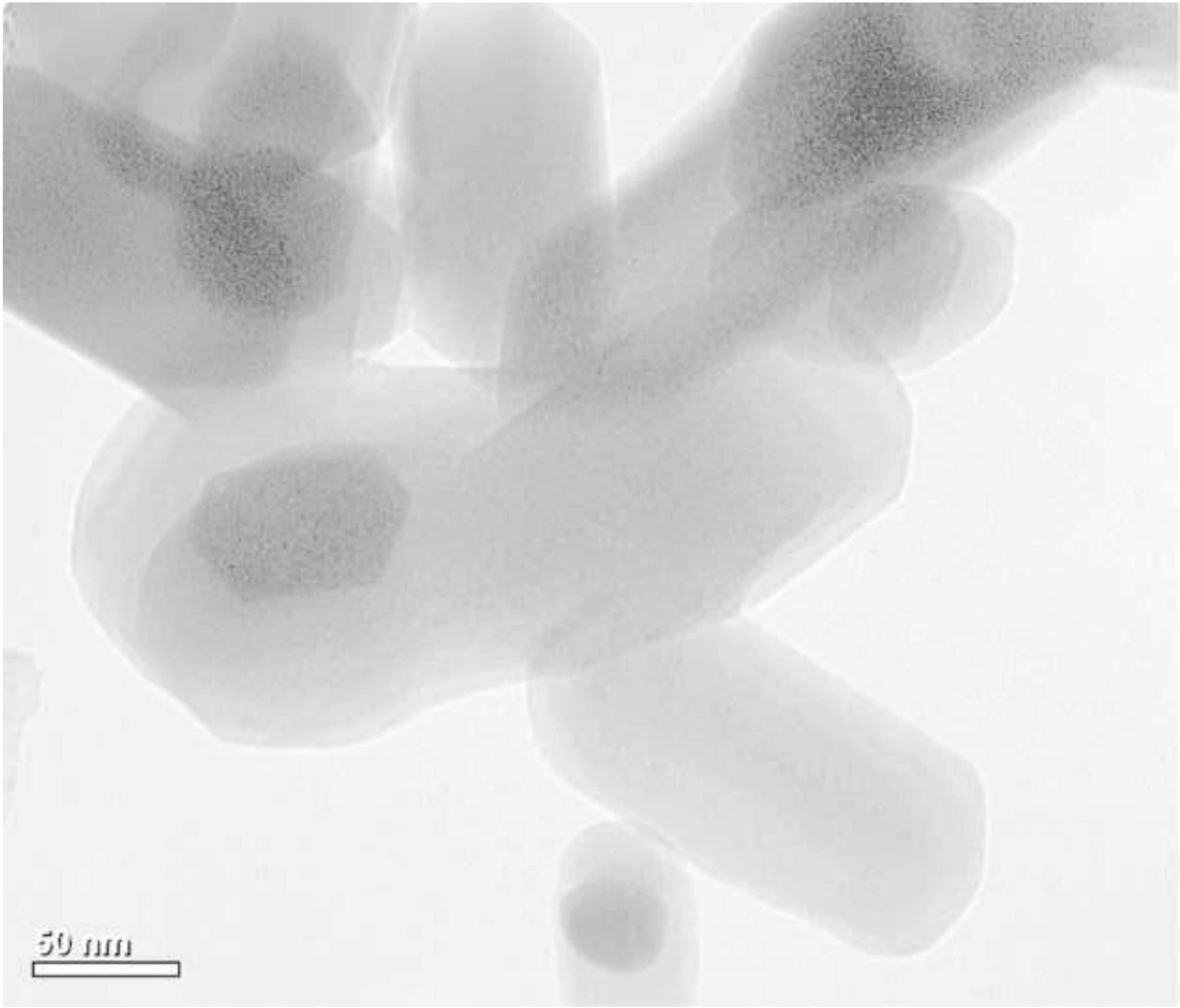

Fig. 2b

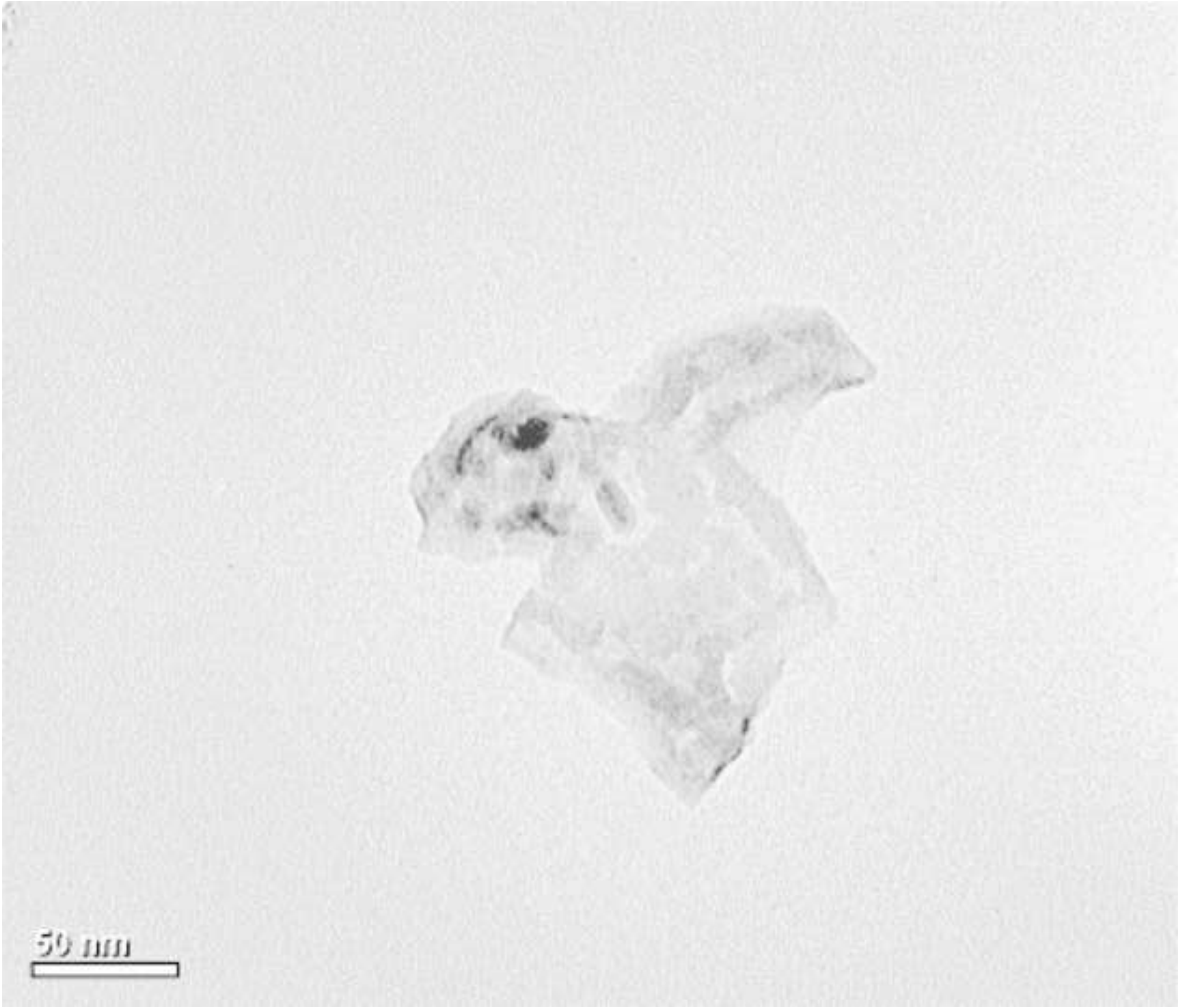

Fig. 2c

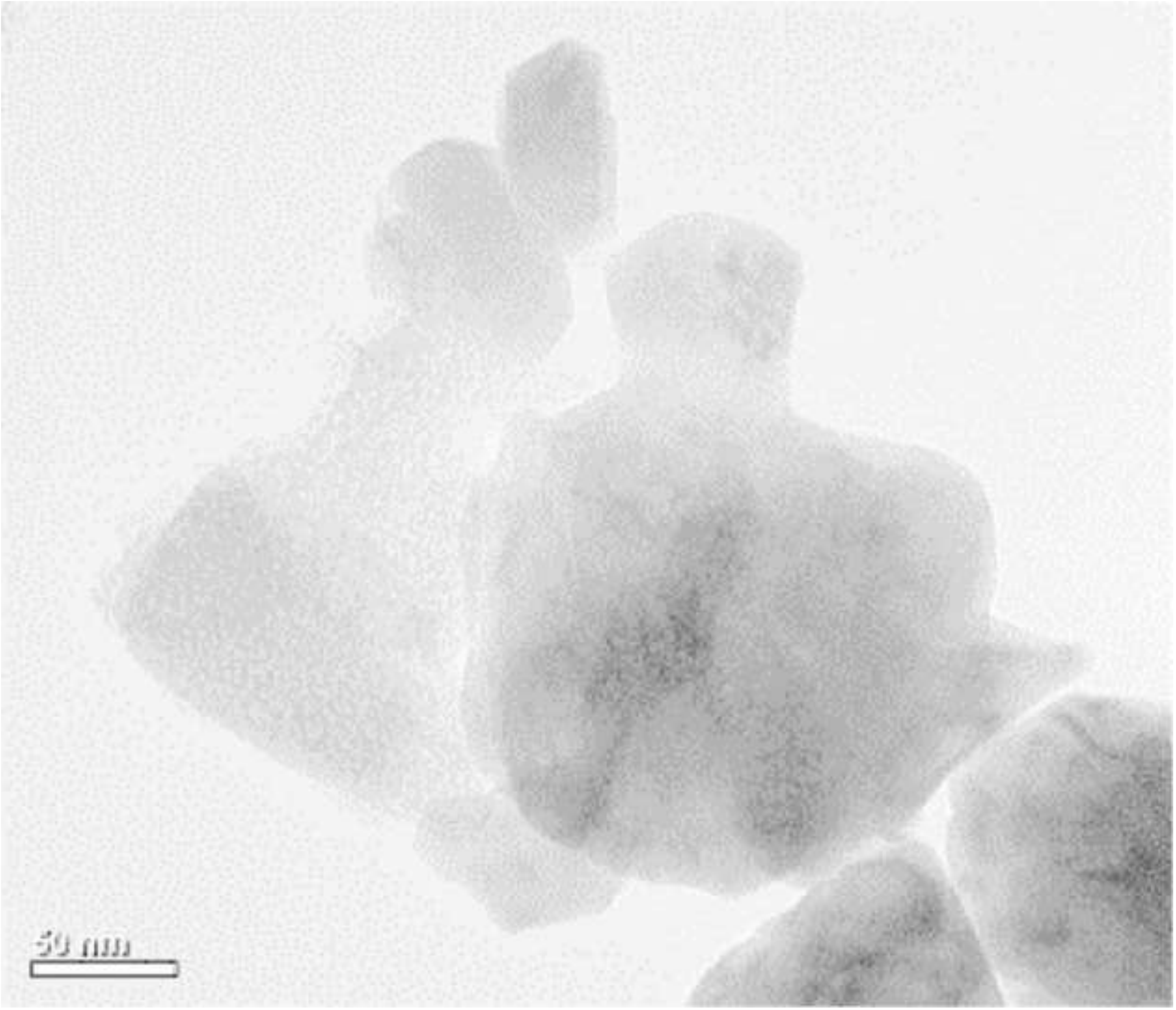

Fig. 2d

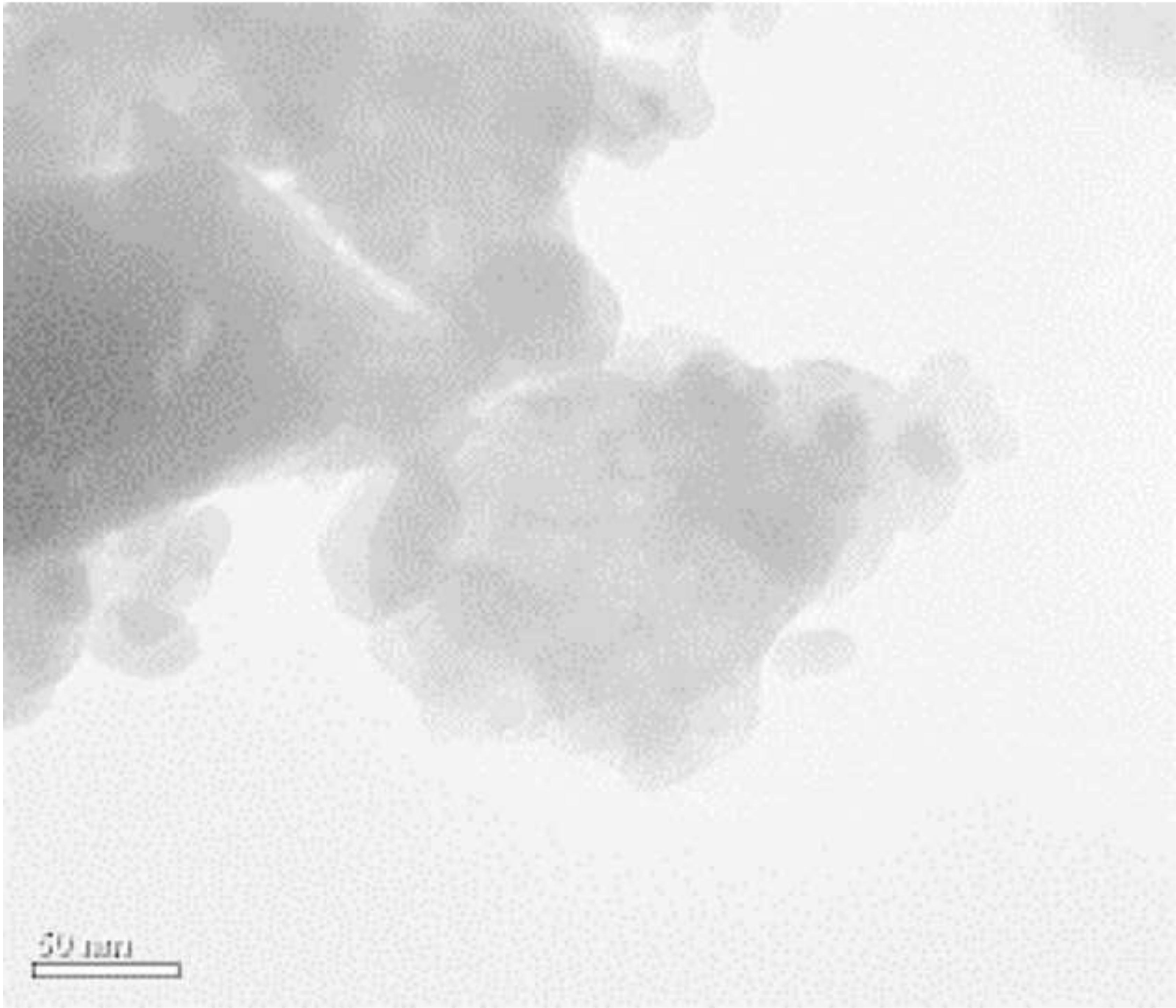

Fig. 3a

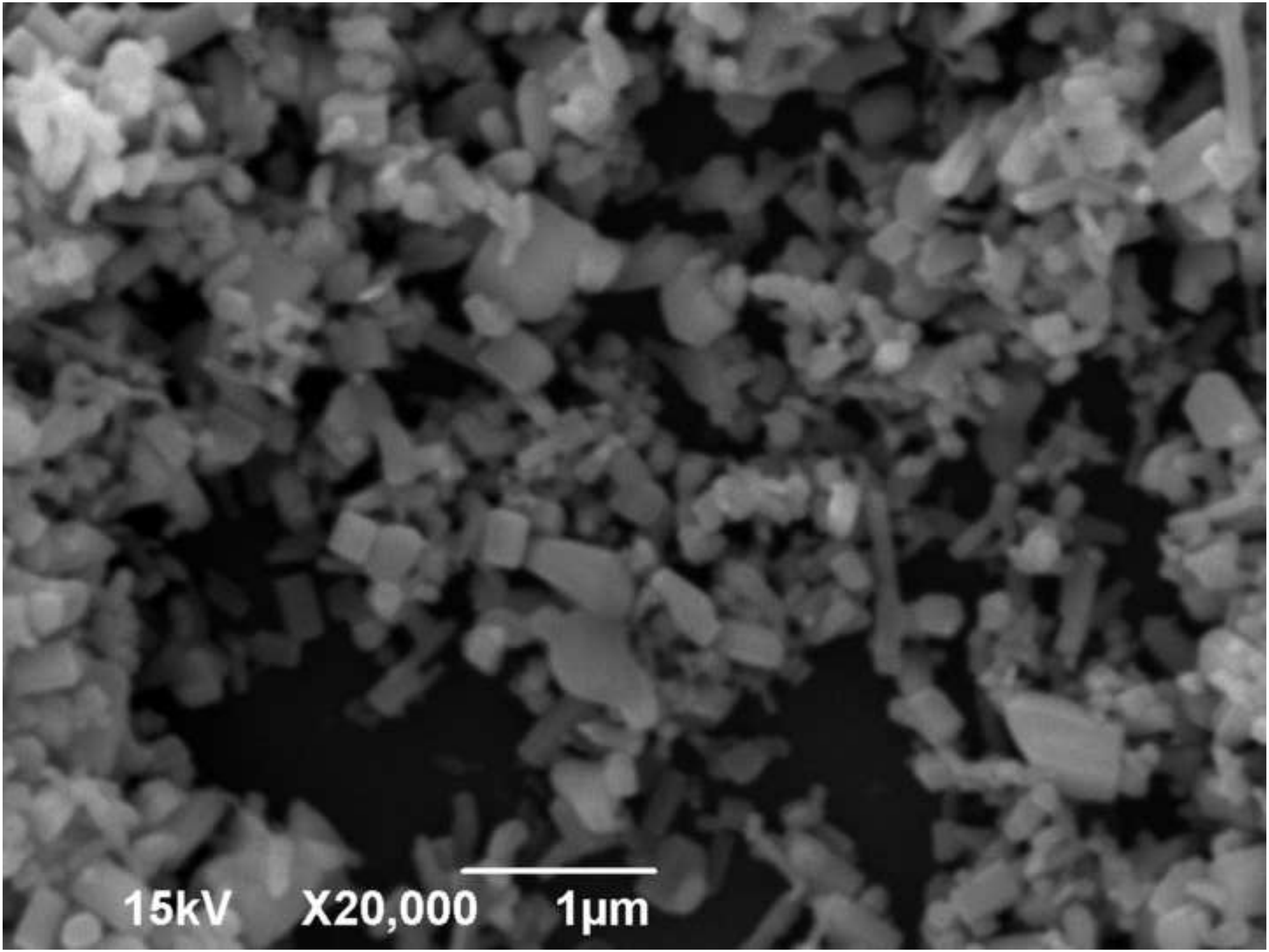
15kV
X20,000
1µm

Fig. 3b

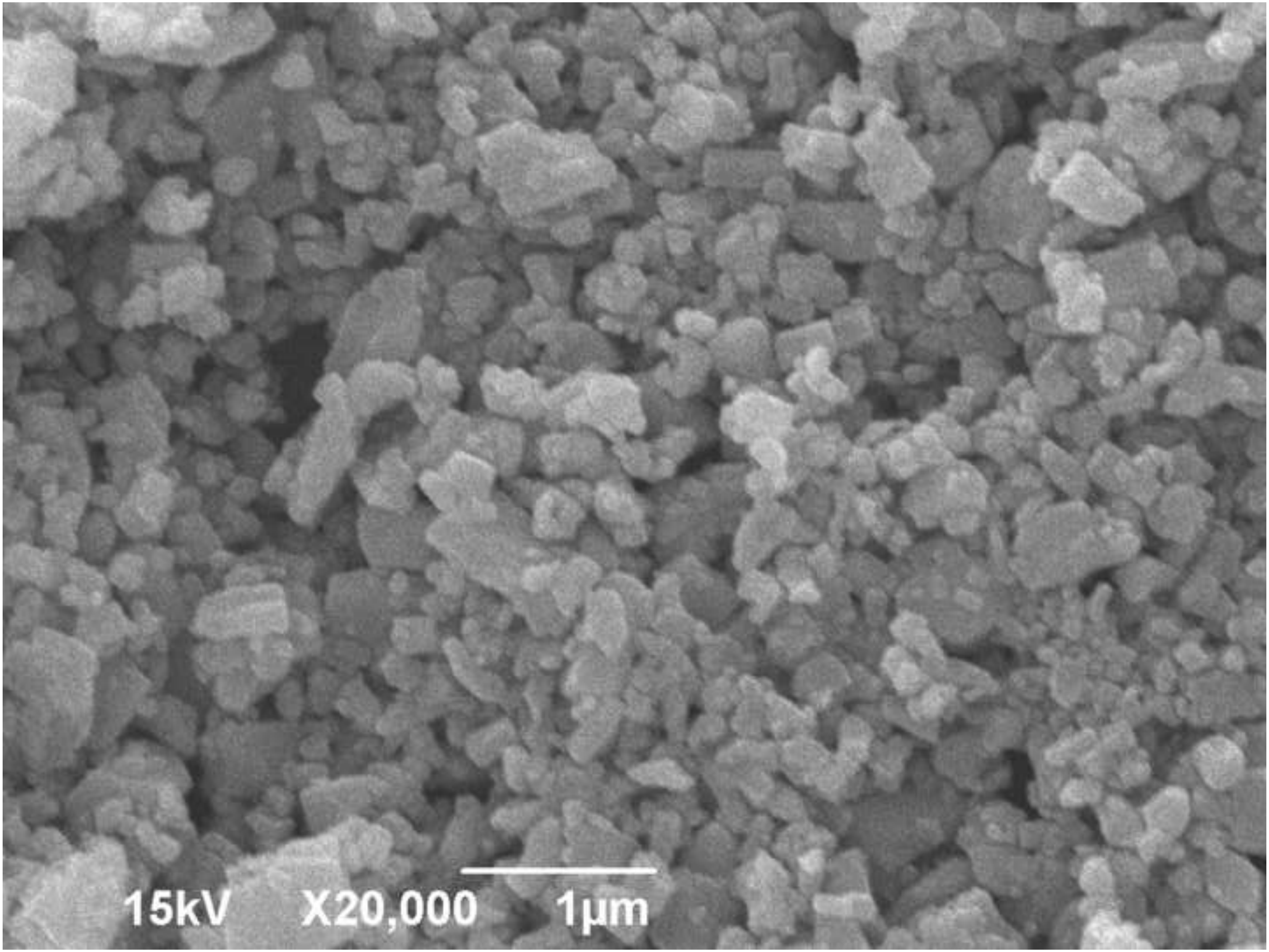
15kV
X20,000
1μm

Fig. 3c

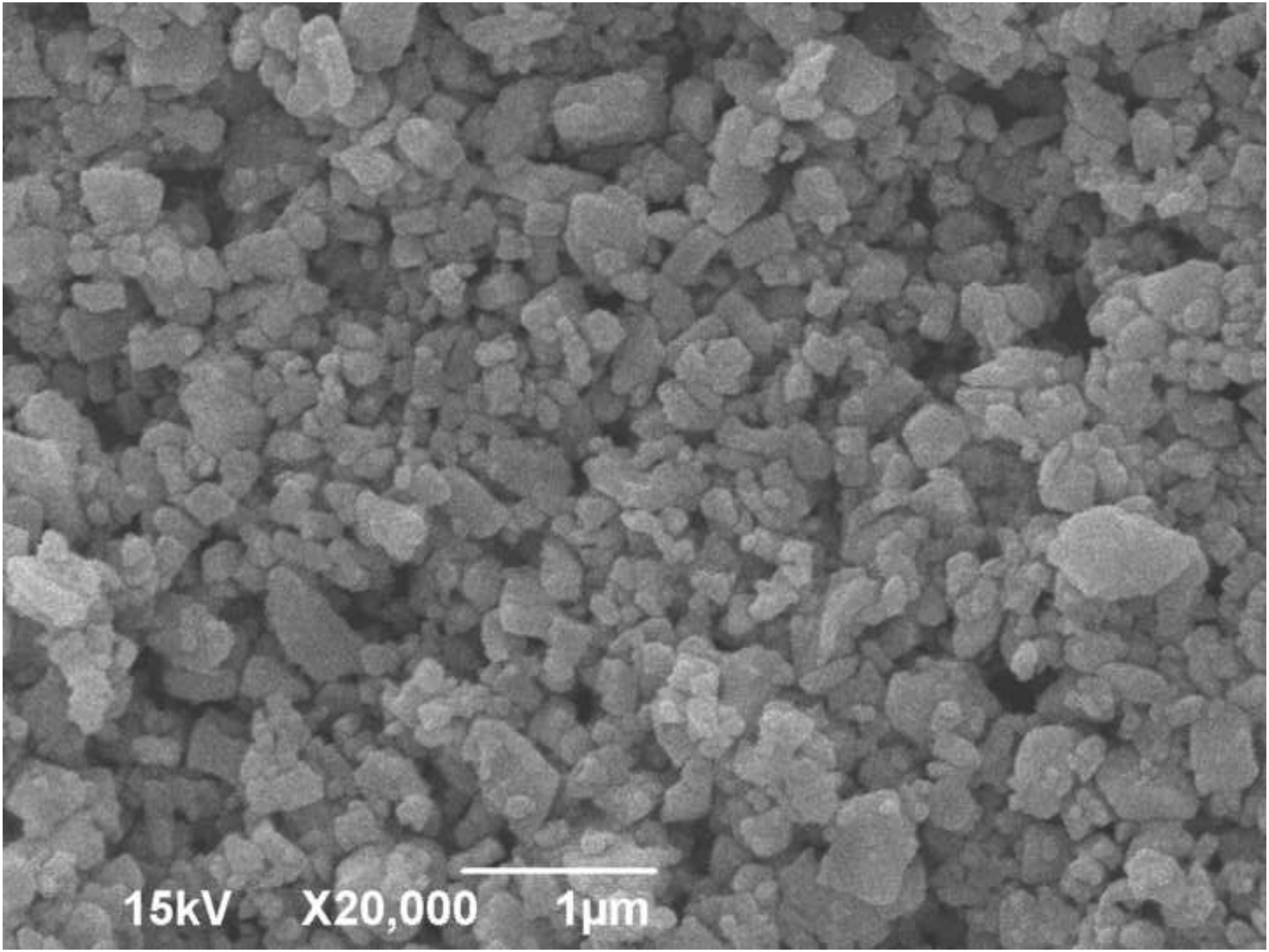
15kV
X20,000
1µm

Fig. 3d

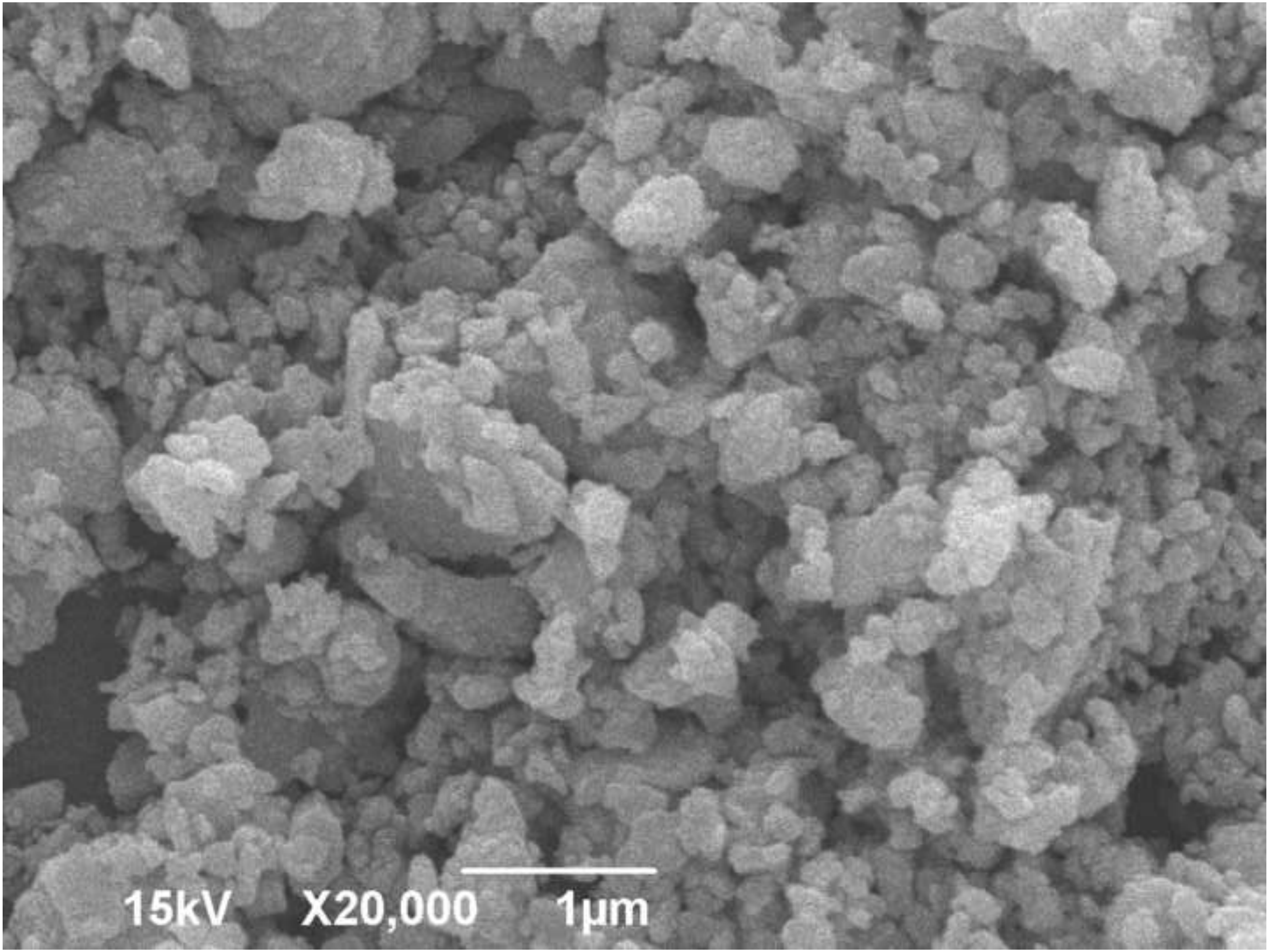
15kV
X20,000
1µm

Fig. 4

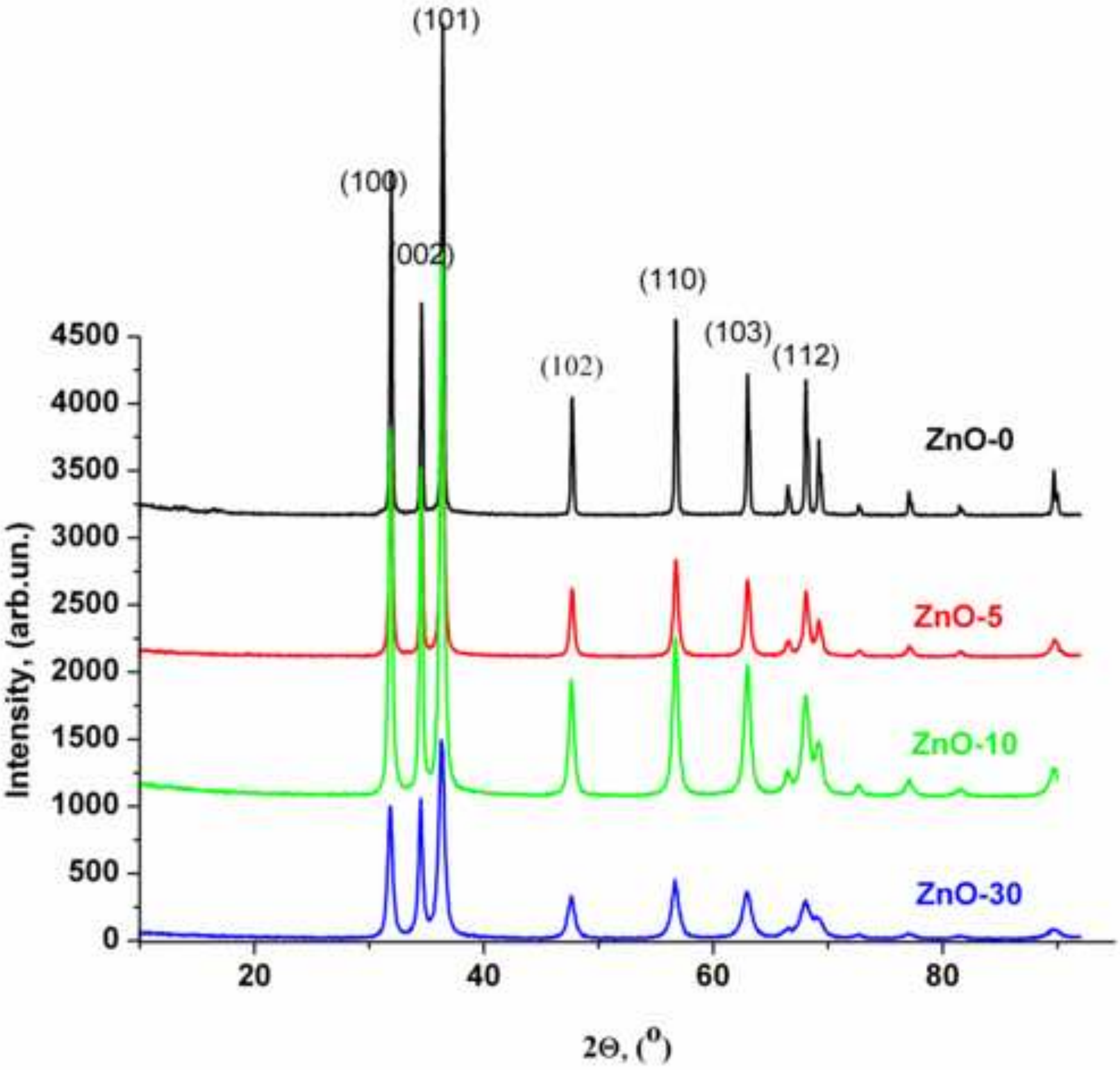
(101)
(100)
(002)
(110)
(103)
(112)
(102)
ZnO-0
ZnO-5
ZnO-10
ZnO-30
Intensity, (arb.un.)
4500
4000
3500
3000
2500
2000
1500
1000
500
0
20
40
60
80
2Θ, (°)

Fig. 5

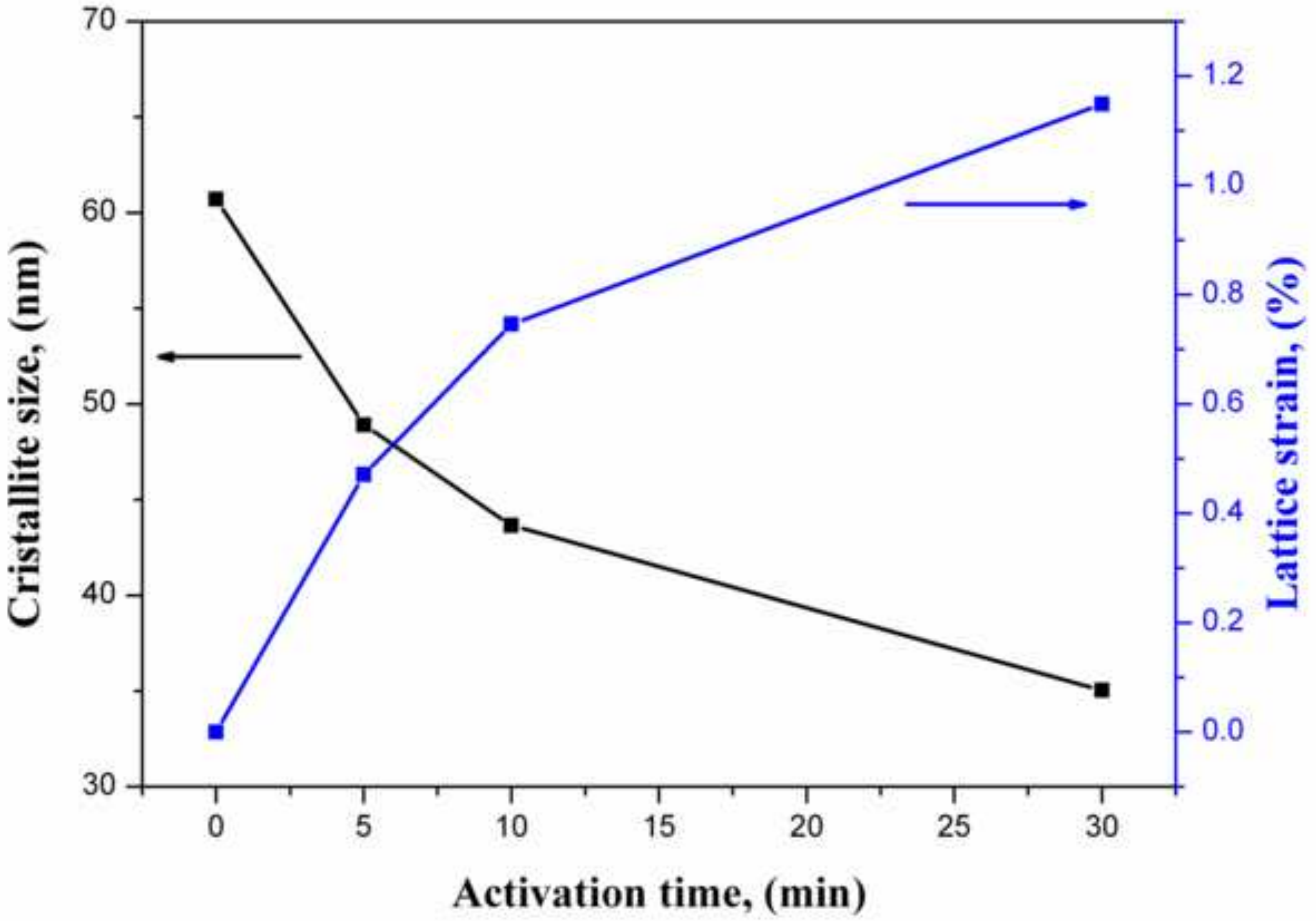
70
60
50
40
30
Cristallite size, (nm)
1.2
1.0
0.8
0.6
0.4
0.2
0.0
Lattice strain, (%)
0
5
10
15
20
25
30
Activation time, (min)

Fig. 6a

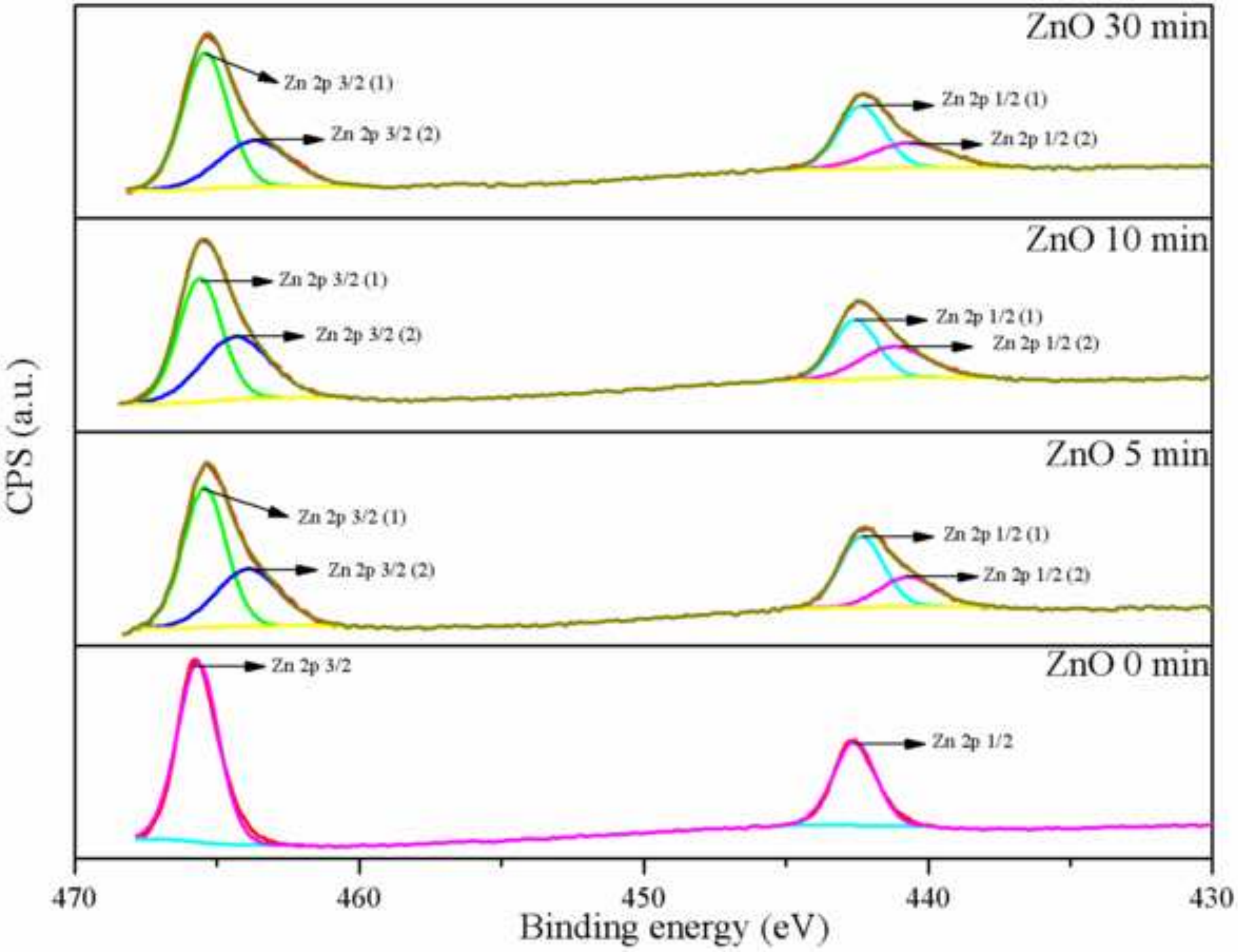
ZnO 30 min
Zn 2p 3/2 (1)
Zn 2p 3/2 (2)
Zn 2p 1/2 (1)
Zn 2p 1/2 (2)
ZnO 10 min
Zn 2p 3/2 (1)
Zn 2p 3/2 (2)
Zn 2p 1/2 (1)
Zn 2p 1/2 (2)
ZnO 5 min
Zn 2p 3/2 (1)
Zn 2p 3/2 (2)
Zn 2p 1/2 (1)
Zn 2p 1/2 (2)
ZnO 0 min
Zn 2p 3/2
Zn 2p 1/2
CPS (a.u.)
470
460
450
440
430
Binding energy (eV)

Fig. 6b

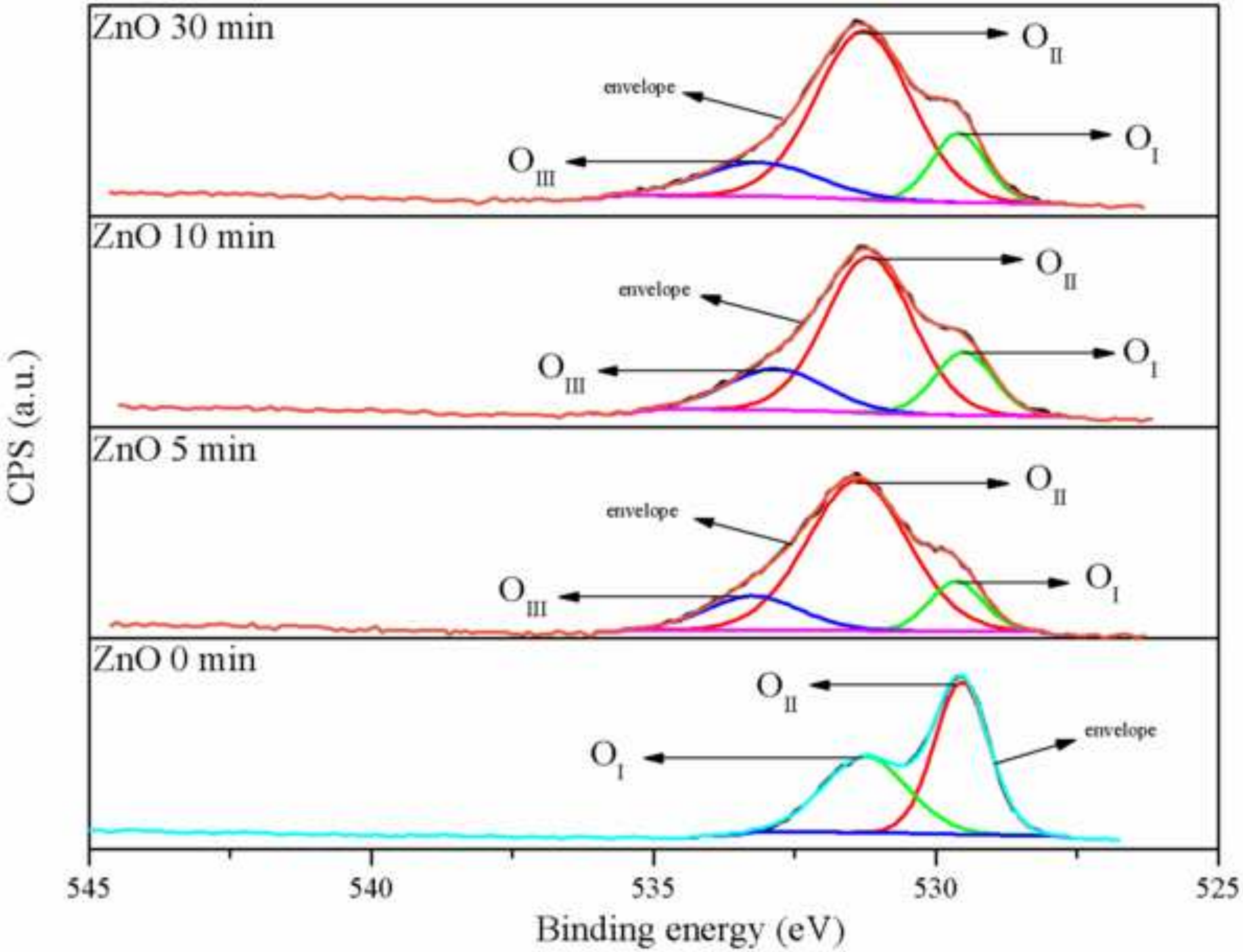
ZnO 30 min
envelope
O_{II}
O_{I}
O_{III}
ZnO 10 min
envelope
O_{II}
O_{I}
O_{III}
ZnO 5 min
envelope
O_{II}
O_{I}
O_{III}
ZnO 0 min
O_{II}
envelope
O_{I}
CPS (a.u.)
545
540
535
530
525
Binding energy (eV)

Fig. 7

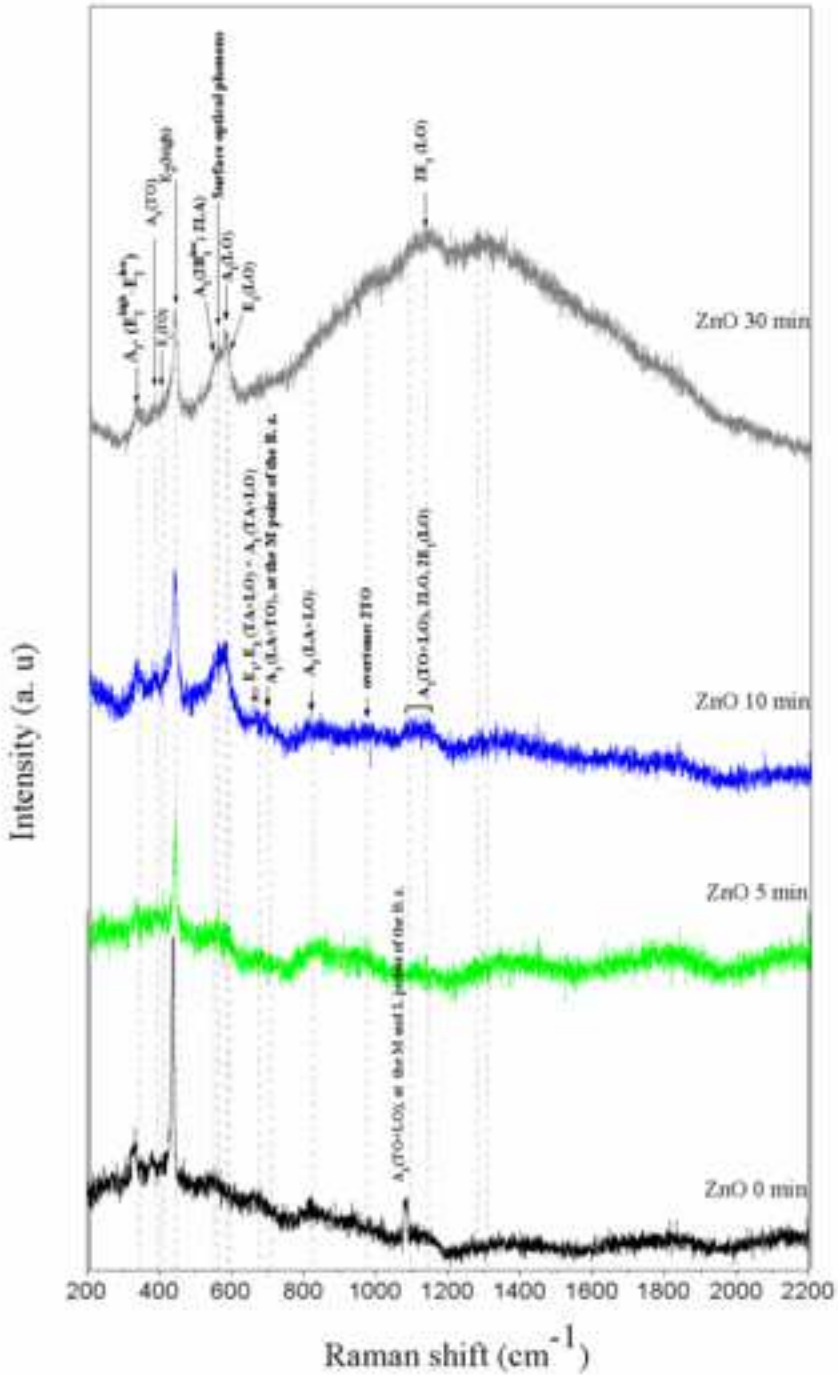
A1, (E2high - E2low)
E1(TO)
A1(TO)
E2(high)
A1(2E1low; 2LA)
Surface optical phonons
A1(LO)
E1(LO)
2E1 (LO)
ZnO 30 min
E1, E2 (TA+LO) + A1(TA+LO)
A1(LA+TO), at the M point of the B. z.
A1(LA+LO)
overtone ITO
A1(TO+LO), 2LO, 2E1(LO)
ZnO 10 min
ZnO 5 min
A1(TO+LO) at the M and L points of the B. z.
ZnO 0 min
Intensity (a. u)
200
400
600
800
1000
1200
1400
1600
1800
2000
2200
Raman shift (cm-1)

Fig. 8

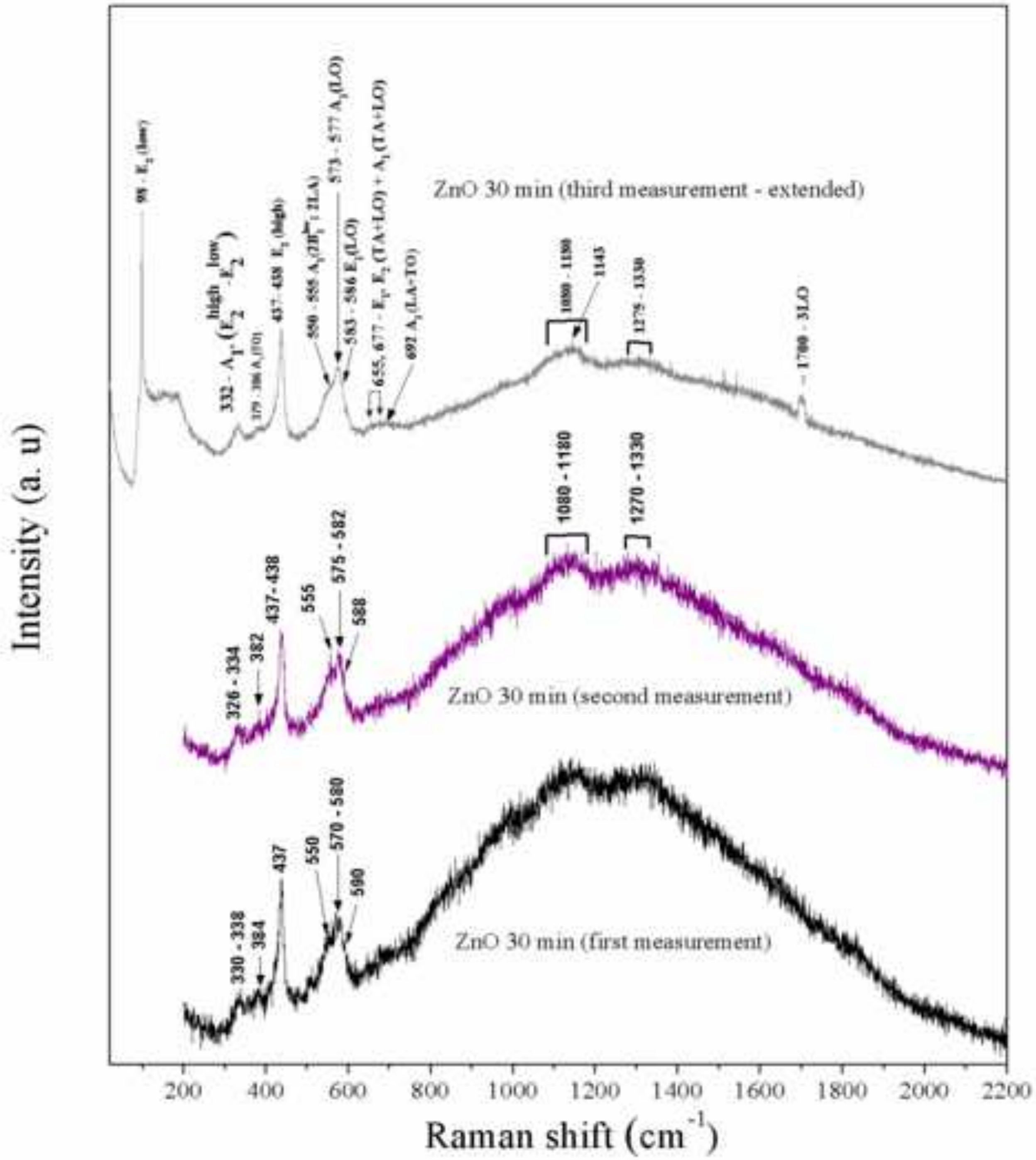
98 - E2 (low)
332 - A1T, (E2high - E2low)
379 - 386 A1(TO)
437 - 438 E2 (high)
550 - 555 A1(2B1low ; 2LA)
573 - 577 A1(LO)
583 - 586 E1(LO)
655, 677 - E1, E2 (TA+LO) + A1(TA+LO)
692 A1(LA-TO)
1080 - 1180
1143
1275 - 1330
1700 - 3LO
ZnO 30 min (third measurement - extended)
1080 - 1180
1270 - 1330
326 - 334
382
437 - 438
555
575 - 582
588
ZnO 30 min (second measurement)
330 - 338
384
437
550
570 - 580
590
ZnO 30 min (first measurement)
Intensity (a. u)
200
400
600
800
1000
1200
1400
1600
1800
2000
2200
Raman shift (cm-1)

Fig. 9

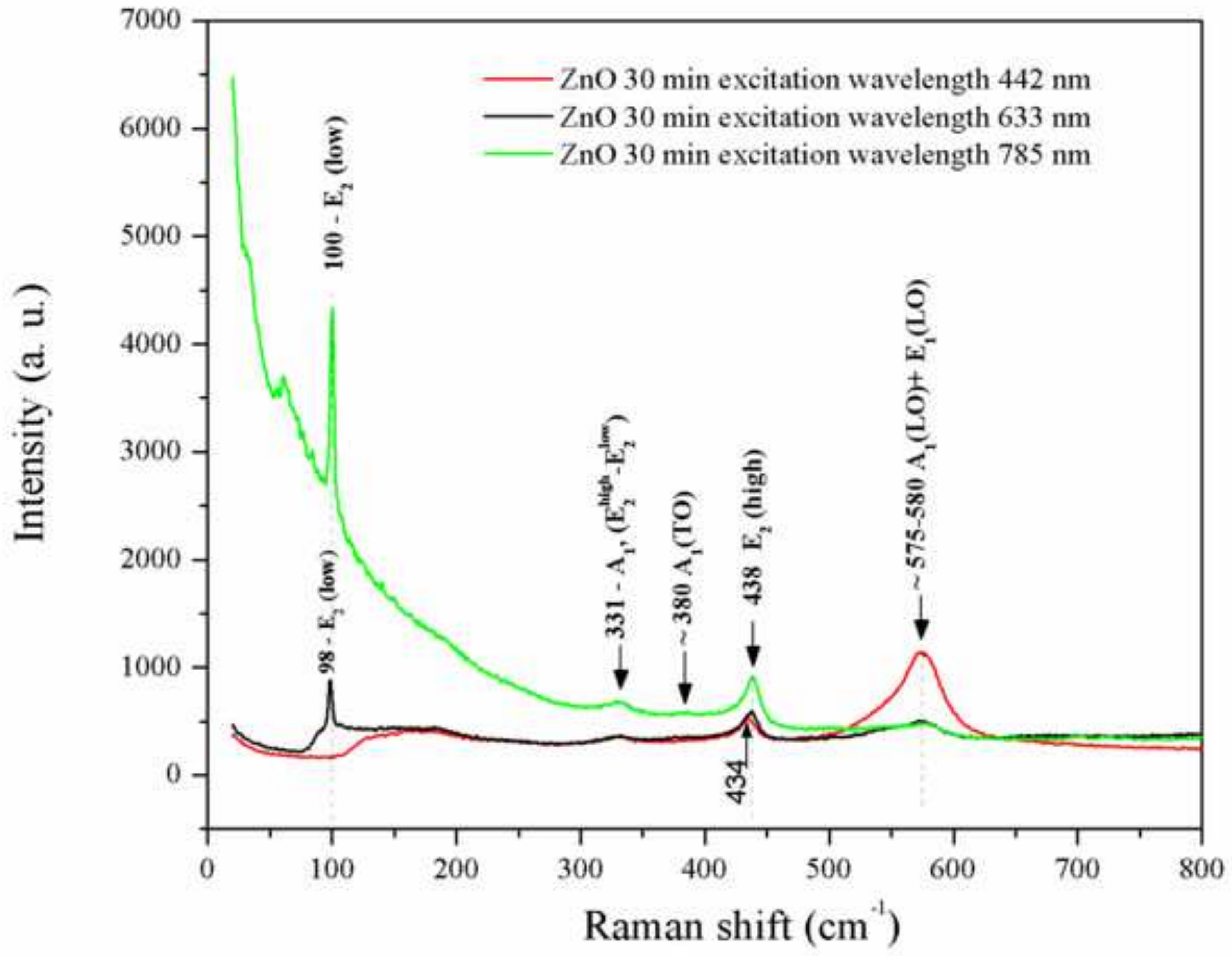
ZnO 30 min excitation wavelength 442 nm
ZnO 30 min excitation wavelength 633 nm
ZnO 30 min excitation wavelength 785 nm
100 - E_2 (low)
98 - E_2 (low)
331 - A_1, (E_2^{high}-E_2^{low})
~ 380 A_1(TO)
438 E_2 (high)
~ 575-580 A_1(LO)+ E_1(LO)
434
Intensity (a. u.)
Raman shift (cm^{-1})
0
1000
2000
3000
4000
5000
6000
7000
0
100
200
300
400
500
600
700
800

Fig. 10

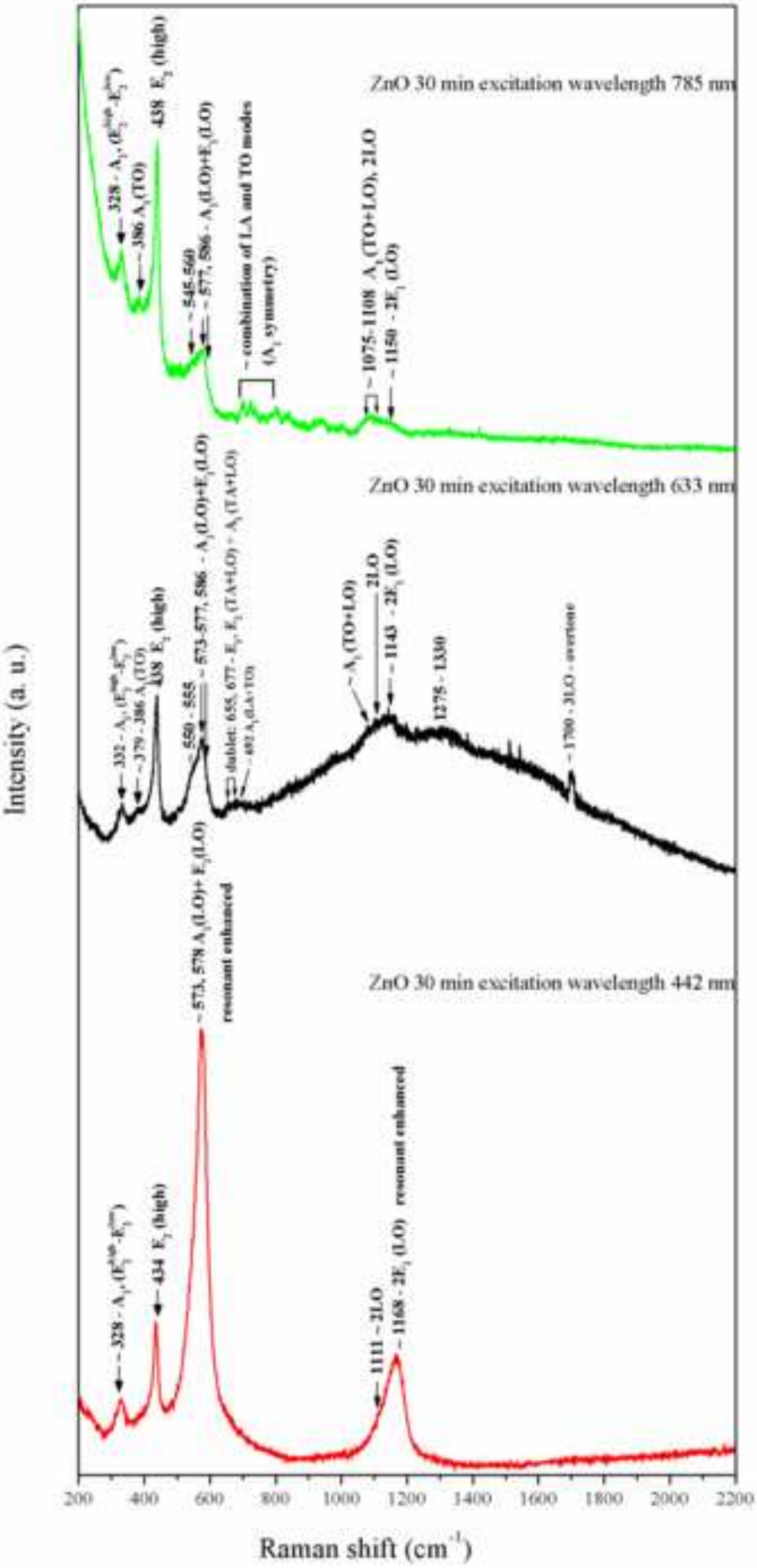
ZnO 30 min excitation wavelength 785 nm
328 - A1, (E2high-E2low)
386 A1(TO)
438 E2 (high)
545-560
577, 586 - A1(LO)+E1(LO)
combination of LA and TO modes (A1 symmetry)
1075-1108 A1(TO+LO), 2LO
1150 - 2E1 (LO)
ZnO 30 min excitation wavelength 633 nm
332 - A1, (E2high-E2low)
379 - 386 A1(TO)
438 E2 (high)
550 - 555
573-577, 586 - A1(LO)+E1(LO)
doublet: 655, 677 - E1, E2 (TA+LO) + A1 (TA+LO)
693 A1(LA+TO)
A1 (TO+LO)
2LO
1143 - 2E1 (LO)
1275 - 1330
1700 - 3LO - overtone
ZnO 30 min excitation wavelength 442 nm
573, 578 A1(LO)+ E1(LO)
resonant enhanced
328 - A1, (E2high-E2low)
434 E2 (high)
1111 - 2LO
1168 - 2E1 (LO)
resonant enhanced
Intensity (a. u.)
200
400
600
800
1000
1200
1400
1600
1800
2000
2200
Raman shift (cm-1)